Article

Developmental Cell

Temporal dynamics and stoichiometry in human Notch signaling from Notch synaptic complex formation to nuclear entry of the Notch intracellular domain

Graphical abstract

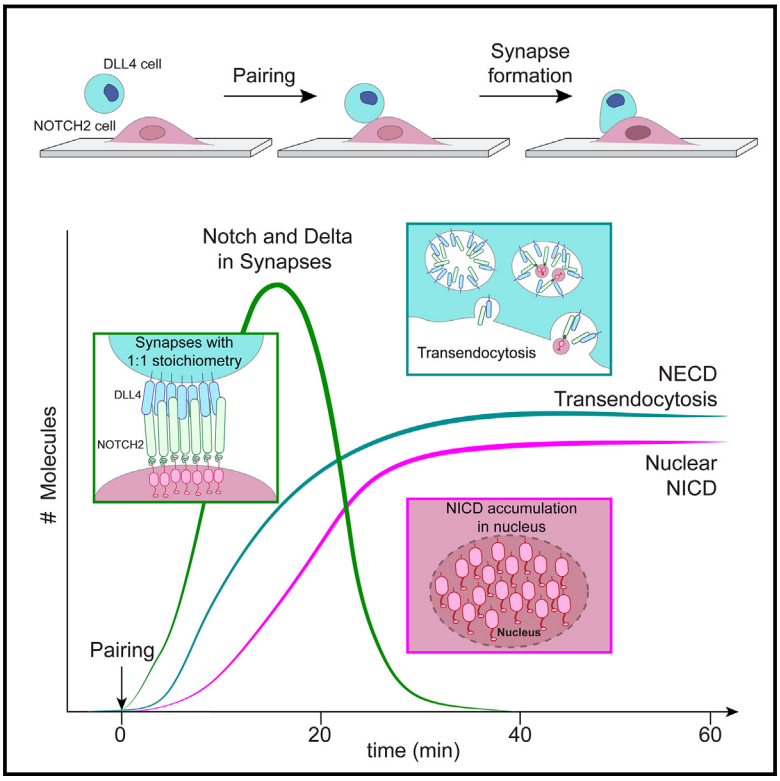

Highlights

- Notch and Delta form synapses with 1:1 stoichiometry at sites of cell-cell contact
- Synapses are transient, resolving after ~20 min of cell contact
- Synapse formation precedes entry of the Notch ectodomain into the Delta cell
- Synapse formation precedes nuclear accumulation of the Notch intracellular domain

Authors

Lena Tveriakhina, Gustavo Scanavachi, Emily D. Egan, ..., Jon C. Aster, Tom Kirchhausen, Stephen C. Blacklow

Correspondence

kirchhausen@crystal.harvard.edu (T.K.), stephen_blacklow@hms.harvard.edu (S.C.B.)

In brief

Tveriakhina, Scanavachi, et al. employed live-cell microscopy to visualize the stoichiometry and dynamics of Notch and Delta at natural protein abundance in sender and receiver cells after contact. This work directly connects Notch-Delta synapse dynamics to Notch ectodomain transendocytosis and Notch intracellular domain nuclear accumulation with spatiotemporal precision.

Tveriakhina et al., 2024, Developmental Cell 59, 1–14
June 3, 2024
https://doi.org/10.1016/j.devcel.2024.03.021

CellPress

Developmental Cell

CellPress

Article

Temporal dynamics and stoichiometry in human Notch signaling from Notch synaptic complex formation to nuclear entry of the Notch intracellular domain

Lena Tveriakhina,[1,8] Gustavo Scanavachi,[2,3,8] Emily D. Egan,[1] Ricardo Bango Da Cunha Correia,[2,3] Alexandre P. Martin,[1] Julia M. Rogers,[1] Jeremy S. Yodh,[5] Jon C. Aster,[6] Tom Kirchhausen,[2,3,4,*] and Stephen C. Blacklow[1,7,9,*]

[1]Department of Biological Chemistry and Molecular Pharmacology, Blavatnik Institute, Harvard Medical School, Boston, MA 02115, USA
[2]Department of Cell Biology, Harvard Medical School, Boston, MA 02115, USA
[3]Program in Cellular and Molecular Medicine, Boston Children's Hospital, Boston, MA 02115, USA
[4]Department of Pediatrics, Harvard Medical School, Boston, MA 02115, USA
[5]Department of Physics, Harvard University, Cambridge, MA 02138, USA
[6]Department of Pathology, Brigham and Women's Hospital, Boston, MA 02115, USA
[7]Department of Cancer Biology, Dana Farber Cancer Institute, Boston, MA 02215, USA
[8]These authors contributed equally
[9]Lead contact
*Correspondence: kirchhausen@crystal.harvard.edu (T.K.), stephen_blacklow@hms.harvard.edu (S.C.B.)
https://doi.org/10.1016/j.devcel.2024.03.021

SUMMARY

Mammalian Notch signaling occurs when the binding of Delta or Jagged to Notch stimulates the proteolytic release of the Notch intracellular domain (NICD), which enters the nucleus to control target gene expression. To determine the temporal dynamics of events associated with Notch signaling under native conditions, we fluorescently tagged Notch and Delta at their endogenous genomic loci and visualized them upon pairing of receiver (Notch) and sender (Delta) cells as a function of time after cell contact. At contact sites, Notch and Delta immediately accumulated at 1:1 stoichiometry in synapses, which resolved by 15–20 min after contact. Synapse formation preceded the entrance of the Notch extracellular domain into the sender cell and accumulation of NICD in the nucleus of the receiver cell, which approached a maximum after ~45 min and was prevented by chemical and genetic inhibitors of signaling. These findings directly link Notch-Delta synapse dynamics to NICD production with spatiotemporal precision.

INTRODUCTION

Notch signaling influences critical cell fate decisions in all metazoans and regulates tissue homeostasis in adults.[1–3] Aberrant Notch signaling is also associated with a variety of human pathologies, such as Alagille syndrome, caused by loss-of-function mutations in *NOTCH2* or *JAGGED1*,[4–6] and the stroke syndrome CADASIL, caused by missense mutations in *NOTCH3*.[7] Oncogenic gain-of-function mutations in human *NOTCH1* are frequently found in human T cell acute lymphoblastic leukemia/lymphoma (T-ALL),[8] B cell malignancies,[9] and solid tumors.[10] Genomic studies have also uncovered loss-of-function mutations of *NOTCH1*, *NOTCH2*, and *NOTCH3* in squamous cell carcinomas,[11,12] and in precancerous regions of sun-exposed skin.[13]

Mammals have four Notch receptors (NOTCH1–4) and four well-characterized activating ligands (DLL1, DLL4, JAG1, and JAG2). Notch proteins are single-pass transmembrane receptors normally processed during maturation by a furin-like protease at an extracellular site called S1[14,15] to generate non-covalently associated extracellular (Notch extracellular domain [NECD]) and transmembrane (NTM) subunits. The mature heterodimeric receptor normally resides on the cell surface of the signal-receiving cell (or receiving cell) in an autoinhibited or ''off'' state and signaling is initiated at sites of cell-cell contact when Notch proteins on a receiver cell bind to Delta or Jagged ligands on a sender cell. Ligand binding relieves Notch autoinhibition by inducing proteolysis by the ADAM10 metalloprotease at a membrane proximal site called S2, producing a truncated transmembrane subunit called NEXT (for Notch extracellular truncation). NEXT becomes a substrate for the intramembrane protease gamma-secretase (γ-secretase), which cleaves Notch at site S3. This proteolytic step releases the Notch intracellular domain (NICD), which enters the nucleus and forms a multiprotein complex with the DNA-binding transcription factor RBPJ, a Mastermind-like family protein (MAML), and additional co-activators to induce Notch target gene transcription.[1,3] The fate of the NECD is less clear, but studies suggest a model in which it is endocytosed into the sender cell in complex with ligand, a process that depends on the E3 ubiquitin ligase Mindbomb (MIB).[16–19]

Although these steps of Notch signaling have been studied since *Drosophila melanogaster* Notch was cloned 40 years ago,[20] how these events are temporally coupled and choreographed during

Please cite this article in press as: Tveriakhina et al., Temporal dynamics and stoichiometry in human Notch signaling from Notch synaptic complex formation to nuclear entry of the Notch intracellular domain, Developmental Cell (2024), https://doi.org/10.1016/j.devcel.2024.03.021

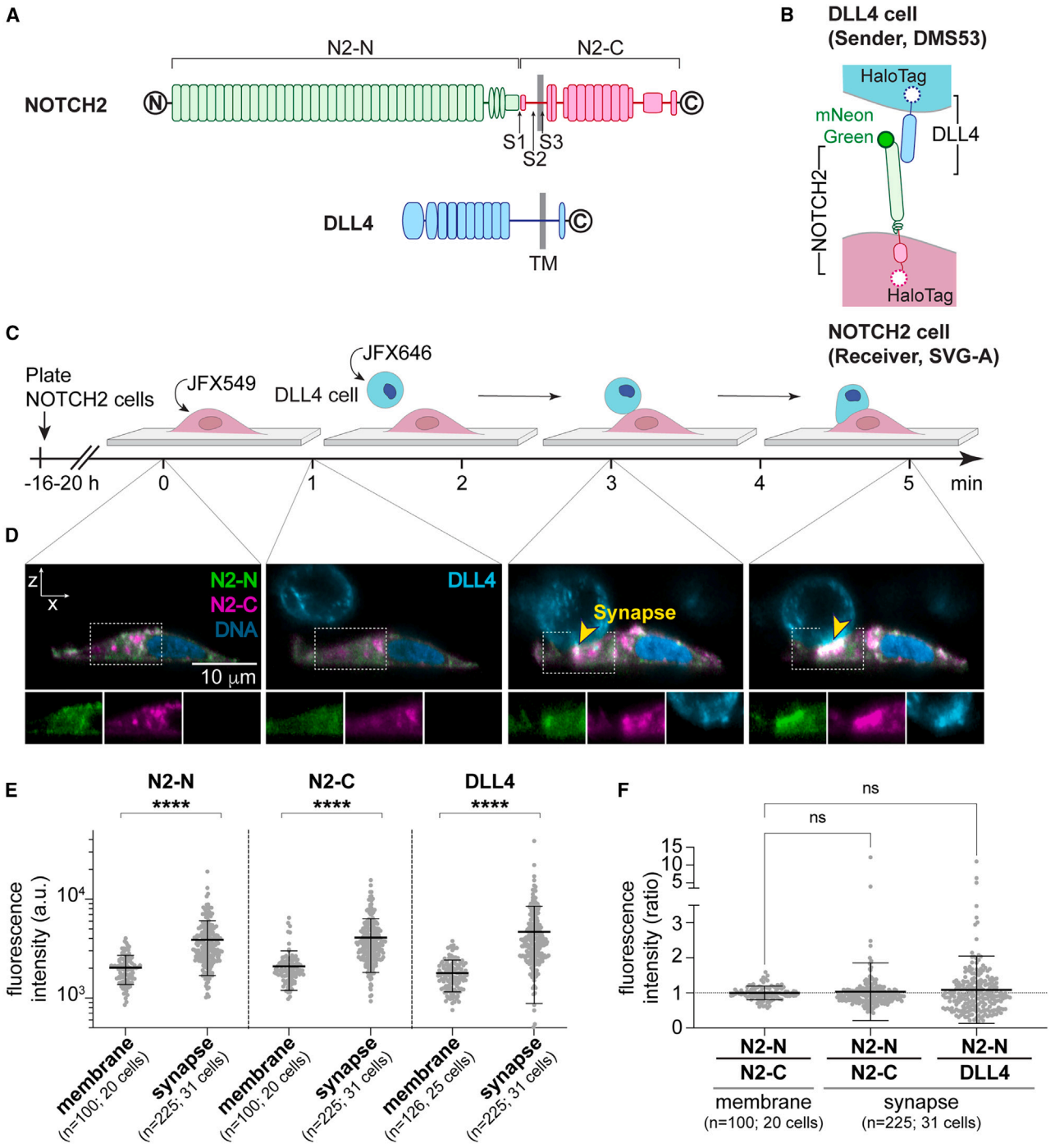

Figure 1. Formation of synapses at sites of NOTCH2-DLL4 contact

(A) Domain organization of NOTCH2 and DLL4. The NOTCH2 extracellular domain (N2-N) is green, the NOTCH2 transmembrane subunit (N2-C) is magenta, and DLL4 is blue. N- and C-terminal tagging sites are shown in black. The sites of NOTCH2 proteolytic cleavage by Furin (S1), ADAM10 (S2), and γ-secretase (S3) are indicated.

(B) Schematic showing the colors of the fluorescent labels used in cell pairing experiments. The N2-N label on NECD is mNeonGreen, the N2-C label on the C terminus is JFX549 coupled to HaloTag (magenta), and the DLL4 C-terminal label is JFX646 coupled to HaloTag (blue).

(C) Cell paring procedure. NOTCH2 and DLL4 cells were separately labeled with JFX549 and JFX646. DLL4 cells were detached and delivered to NOTCH2 cells, and cell pairing was monitored by spinning disk confocal or lattice light-sheet microscopy.

(D) Representative lattice light-sheet images (orthogonal view, despeckled) showing NOTCH2 cells before (0 min) and 1, 3, and 5 min after microfluidic delivery of DLL4 cells pre-treated with anti-DLL1, anti-JAG1, and anti-JAG2 blocking antibodies. N2-N is colored green, N2-C is magenta, DLL4 is cyan, and DNA is pseudocolored blue. Yellow arrowhead: synapse. Single channels are also shown as insets. Scale bars, 10 μm.

(legend continued on next page)

Please cite this article in press as: Tveriakhina et al., Temporal dynamics and stoichiometry in human Notch signaling from Notch synaptic complex formation to nuclear entry of the Notch intracellular domain, Developmental Cell (2024), https://doi.org/10.1016/j.devcel.2024.03.021

signaling is less well understood. Likewise, it is not known what the receptor-ligand stoichiometry is when complexes form at the membrane, nor is it clear how efficiently ligand-receptor engagement at the membrane leads to NICD production. Moreover, time-resolved linkage of the ligand-receptor interaction to internalization of NECD into sender cells has not been directly observed.

Using fluorescence microscopy in fly or mammalian cells transiently or stably overexpressing ligand and/or receptor molecules, others have shown that at sites of direct cell-cell contact, Notch and its ligands can gather and form stable clusters.[21–25] Similarly, transendocytosis of the NECD into vesicular structures within sending cells has also been observed in cell culture and in flies.[23,26] Ectopic overexpression of Notch can also result, however, in intracellular retention, mislocalization, and clustering of receptor molecules within the endoplasmic reticulum (ER),[27–29] raising the possibility that these findings are not physiologically representative. It is therefore important to use tagged Notch proteins expressed from endogenous loci to ensure faithful recapitulation of the temporal dynamics of early events responsible for Notch signaling.

In the quantitative studies reported here, we combined use of volumetric spinning disk confocal and lattice light-sheet microscopy (LLSM)[30] to image cells expressing physiological amounts of fluorescently tagged Notch and ligand proteins expressed from their endogenous loci to analyze protein localization, organization, and dynamics in living cells. LLSM was chosen because it minimizes photobleaching, increases signal to noise ratio, and allows for high spatiotemporal precision of time series recorded from the whole cell volume. When sender and receiver cells made contact, ligands and receptors clustered into synapses at the contact site, with a synapse lifetime of roughly 15–20 min and a ligand:receptor stoichiometry of 1:1. Synapse formation preceded transendocytosis of NECD (and some full-length Notch) into the sending cell and eventual accumulation of up to 2,000 NICD molecules in the nucleus of the receiving cell. This work defines the stoichiometry and integrated temporal order and timing of central steps in Notch signal transduction from synapse formation through nuclear NICD accumulation and charts a course for studying real-time Notch-dependent signaling dynamics in living cells in both physiological and pathophysiological contexts.

RESULTS

Establishment of a system to visualize Notch signaling in real time

To study the events of physiologic Notch signaling using fluorescence microscopy in living cells, we screened for Notch- and ligand-expressing cell lines that (1) were amenable to CRISPR-Cas9 engineering, (2) expressed one receptor or ligand endogenously at substantially greater natural abundance than others, and (3) were active as either receiver (Notch-expressing cells) or sender (ligand-expressing cells) cells, as assessed by assays for induction of Notch-dependent gene expression.

SVG-A immortalized fetal astrocytes met these criteria as a Notch (receiver) cell line. They have been successfully engineered using CRISPR-Cas9,[31] express vastly more *NOTCH2* than other Notch isoforms (as judged by analysis of mRNA abundance by quantitative reverse-transcriptase PCR[32]), and exhibit strong induction of a Notch-responsive luciferase reporter gene when co-cultured with U2OS cells ectopically expressing DLL4 (Figure S1A, related to Figure 1). The reporter response was blocked by treatment with a γ-secretase inhibitor (GSI; compound E) and not observed in co-culture assays with parental U2OS cells. The transcriptional response of SVG-A cells to ligand-expressing cells was also greatly reduced when *NOTCH2* was knocked out using CRISPR-Cas9 (Figure S1A, related to Figure 1), confirming that NOTCH2 was responsible for most Notch signaling activity in these cells. Importantly, when SVG-A cells were plated in tissue culture dishes containing immobilized JAG1, sentinel Notch target genes were induced within 2–4 h, and the "Notch signaling pathway" Gene Ontology term[33,34] was enriched among genes induced at 2, 4, and 24 h after stimulation (Figure S1B, related to Figure 1).

We identified two ligand (sender) cell lines that met our criteria. The first sender line was DMS53, which expresses DLL4 as its predominant ligand and activates Notch in SVG-A receiver cells (Figure S1, related to Figure 1). Knockout of DLL4 in DMS53 cells also reduced signal-sending activity (Figure S1J, related to Figure 1), with residual ligand activity likely resulting from the expression of other ligands (Figures S1C and S1D, related to Figure 1). The second sender line was A673, which endogenously expresses JAG1 as its predominant ligand (Figure S2, related to Figure 1) and induces a Notch reporter response in SVG-A receiver cells (Figure S2C, related to Figure 1). Knockout of JAG1 in A673 cells abrogated signal-sending activity (Figure S2H, related to Figure 1), consistent with the observation that JAG1 was the only ligand detectable in these cells by flow cytometry (Figures S2A and S2B, related to Figure 1).

We used CRISPR-Cas9 in SVG-A, DMS53, and A673 cells to fuse fluorescent proteins or HaloTags[35] to Notch and ligand proteins in their endogenous loci for expression at natural abundance. In SVG-A cells, NOTCH2 was double-tagged with mNeonGreen (mNeon)[36] inserted after the signal peptide to position it extracellularly at the mature N terminus of the NECD subunit, and with a HaloTag inserted after A2471 to place a second fluorophore intracellularly at the C terminus of the NTM subunit (Figure 1A; Figure S3, related to Figure 1). These labeling positions are hereafter specified as N2-N and N2-C, respectively. In DMS53 and A673 cells, a HaloTag was fused to the C-terminal end of DLL4 or JAG1, respectively (Figures 1A and 1B; Figures S1F–S1H and S2D–S2F, related to Figure 1). The steady-state amount and signaling activity of tagged receptor and ligand proteins were not substantially altered when compared with endogenous proteins in parental cells,

(E) Fluorescence intensities of N2-N, N2-C, and DLL4 signals in the regions outside of cell-cell contact (membrane) and in synapses.
(F) Ratios of fluorescence intensities of signals associated with N2-N and N2-C in the membrane and of N2-N and N2-C or N2-N and DLL4 in synapses, respectively. Data are represented as mean ± standard deviation; statistical analysis for each pair was performed using Mann-Whitney (E) and Kruskal-Wallis (F) tests; ****$p < 0.0001$; ns, not significant; n, number of synapses and number of cells analyzed as indicated. Regions without any inhomogeneities were selected for membrane analysis to avoid possible autofluorescent puncta.
See also Figures S1–S4.

Please cite this article in press as: Tveriakhina et al., Temporal dynamics and stoichiometry in human Notch signaling from Notch synaptic complex formation to nuclear entry of the Notch intracellular domain, Developmental Cell (2024), https://doi.org/10.1016/j.devcel.2024.03.021

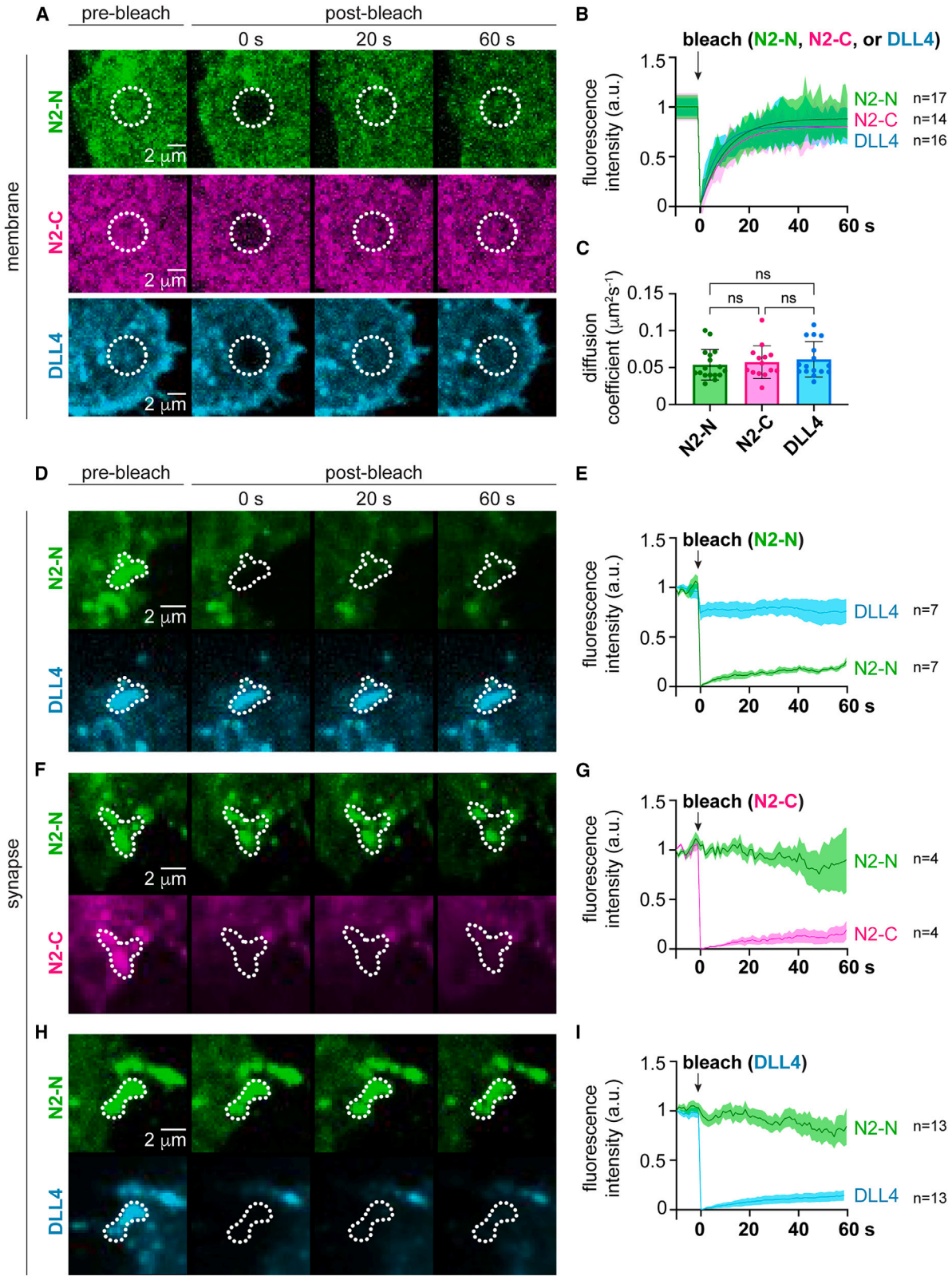

Figure 2. NOTCH2 and DLL4 in synapses do not readily exchange

(A) Fluorescence recovery after photobleaching (FRAP) experiment, showing representative spinning disk confocal images of free N2-N, N2-C, and DLL4 before and as a function of time after photobleaching. Dotted circles indicate photobleached membrane regions used for analysis.

(legend continued on next page)

Please cite this article in press as: Tveriakhina et al., Temporal dynamics and stoichiometry in human Notch signaling from Notch synaptic complex formation to nuclear entry of the Notch intracellular domain, Developmental Cell (2024), https://doi.org/10.1016/j.devcel.2024.03.021

confirming that the tags do not disrupt protein processing or function (Figures S1I–S1L, S2G–S2J, and S3E–S3H, related to Figure 1).

We engineered a microfluidics device for imaging in a confocal (SD) or lattice light-sheet microscope (LLSM). The device made it possible to pair cells and observe the cell pairs in real time from the moment of initial contact, allowing us to follow the dynamics of NOTCH2 and DLL4 associated with signal transmission (Figure 1C; Figures S4A–S4C, related to Figure 1). Sender and receiver cells were separately labeled with HaloTag ligands conjugated to different JaneliaFluorX (JFX) dyes[37] prior to pairing. The sender cells were then delivered to receiver cells pre-plated on the cover slip by passage through a microfluidic chip using a pressure-controlled pump.

Notch synapses form between NOTCH2 and DLL4 at sites of cell-cell contact

In cultured SVG-A cells, NOTCH2 was found at the plasma membrane and in intracellular puncta (Figure 1D; Figure S4D, related to Figure 1) that likely represent trafficking vesicles and/or organelles related to protein synthesis and degradation. The concurrent presence of nonspecific or autofluorescence signals in the green (488) and red (561) channels, also seen as small intracellular puncta in both parental cells and in knockin cells that did not have a JFX dye coupled to the HaloTag (Figures S4D and S4E, related to Figure 1), prevented unambiguous identification of NOTCH2-containing vesicles inside these cells.

To ensure that contact sites between sender and receiver cells included only DLL4 and NOTCH2, we preincubated the DMS53 cells with blocking antibodies[38,39] to prevent DLL1, JAG1, or JAG2 from binding to NOTCH2. These pre-treated DMS53 sender cells delivered to the SVG-A receiver cells then allowed real-time imaging of DLL4 engagement with NOTCH2 at sites of contact (Figures 1C and 1D). The contact sites, which we defined as Notch synapses, showed accumulation of NOTCH2 and DLL4 and presumably occurred at sites of molecular contact between the ectodomains of DLL4 and NOTCH2 (Figure 1D; Videos S1 and S2). Synapses formed with 100% efficiency (i.e., percentage of cell pairs that formed at least one synapse) within seconds every time these two cell types made direct contact under these conditions (Figure S2N, related to Figure 1) and varied in size and shape (Figure S4F, related to Figure 1). Similarly, DLL4 knockout DMS53 cells devoid of DLL4 still formed Notch synapses, mediated by the binding of other ligands to NOTCH2 (Figure S4G, related to Figure 1). Preincubation of parental DMS53 cells with ligand-blocking antibodies to all four canonical ligands (DLL1, DLL4, JAG1, and JAG2),[38–40] however, prevented synapse formation and effectively silenced signaling (Figures S4H and S4I, related to Figure 1), indicating that synapse formation required direct ligand-receptor binding.

To evaluate whether ligand and receptor proteins concentrated at points of cell-cell contact, we compared the fluorescence intensities of the N2-N, N2-C, and DLL4 tags in synapses with their intensities in membrane regions excluded from the synapses ("membrane") and measured significantly higher fluorescence intensity signals in the synapses (Figure 1E). The surface density of receptor and ligand molecules outside of the synapse was not detectably altered upon synapse formation, and less than 5% of the total surface NOTCH2 and DLL4 accumulated in the synapses.

We determined the ratio of fluorescence intensities of the N2-N and N2-C tags in the membrane of receiving cells (before delivery of ligand cells) and set the value of that ratio to a stoichiometry of 1:1 because both fluorophores are coupled to the same receptor protein. The same 1:1 stoichiometry was observed outside synapses after Notch cells contacted sender cells (Figure 1F; N2-N/N2-C in membrane). The N2-N:N2-C stoichiometry remained 1:1 in synapses associated with NOTCH2—DLL4 engagement (Figure 1F; N2-N/N2-C in synapse). To determine the stoichiometric ratio of NOTCH2 to DLL4 in synapses, we exploited the capacity of the HaloTag to be labeled with different dyes and exchanged the Notch C-terminal and DLL4 fluorophores to determine the NOTCH2:DLL4 ratio in the synapse. We established that the N2-N to N2-C and N2-N to DLL4 fluorescent tag ratios were 1:1 independent of the dyes exchanged and indistinguishable from each other (Figure 1F; N2-N/N2-C and N2-N/DLL4 in synapse).

Similarly, a 1:1 receptor:ligand stoichiometry was present at synapses formed by NOTCH2 and JAG1 upon pairing A673 JAG1-HaloTag cells and NOTCH2-tagged SVG-A cells (Figures S2L and S2M, related to Figure 1). One detectable difference was that the A673 (JAG1) cells formed synapses less efficiently than the DMS53 (DLL4) cells (Figure S2N, related to Figure 1), most likely because the amount of JAG1 on the surface of A673 cells was lower than the amount of DLL4 on DMS53 cells. In each case, endogenously expressed ligands and receptors formed synapses at contact sites in living cells with a stoichiometry of 1:1.

NOTCH2 and DLL4 in synapses do not readily exchange

We performed fluorescence recovery after photobleaching (FRAP) in a spinning disk confocal microscope to assess the dynamics of receptor and ligand exchange on the cell surface, both in regions outside of and within synapses. FRAP was performed within a region of interest (ROI) and recovery was monitored at 1 s intervals for a total of 60 s. Outside sites of cell contact, the fluorescence intensity after bleaching recovered 80%–90% of the initial value after 60 s for both the N2-N and N2-C tags and for the DLL4 tag, indicating that both proteins are mobile on the cell surface (Figures 2A and 2B). The half-times for recovery ($t_{1/2}$) of N2-N and N2-C on SVG-A cells were 7.6 ± 2.5 and 7.2 ± 3.0 s, which correspond to diffusion coefficients (D) of 0.054 ± 0.02 and 0.057 ± 0.02 $\mu m^2\ s^{-1}$, respectively (Figures 2B and 2C). Free

(B) Recovery plots of fluorescence intensity and fitted single exponential curves after photobleaching for N2-N (green), N2-C (magenta), and DLL4 (blue) freely dispersed in the membrane.

(C) Diffusion coefficients derived from FRAP for N2-N (green), N2-C (magenta), and DLL4 (blue) freely dispersed in the membrane.

(D, F, and H) FRAP experiment in synapses, showing representative images of N2-N (D), N2-C (F), and DLL4 (H) before and as a function of time after photobleaching. Images also show unbleached fluorophores (DLL4 in D, N2-N in F, and N2-N in H) as a positional reference for the synapses. Areas used for analysis of recovery are represented by dotted lines.

(E, G, and I) FRAP recovery plots for N2-N (E), N2-C (G), and DLL4 (I) when engaged in synapses. Fluorescence intensity of unbleached components of the synapse (DLL4 in E, N2-N in G, and N2-N in I) were also monitored and analyzed as reference. Data are represented as mean ± standard deviation; statistical analysis in (C) was performed using Kruskal-Wallis ANOVA; ns, not significant; n, number of regions/synapses analyzed as indicated. Scale bars, 2 μm.

Please cite this article in press as: Tveriakhina et al., Temporal dynamics and stoichiometry in human Notch signaling from Notch synaptic complex formation to nuclear entry of the Notch intracellular domain, Developmental Cell (2024), https://doi.org/10.1016/j.devcel.2024.03.021

DLL4 molecules on the surface of DMS53 cells had a similar mobility, with a recovery $t_{1/2}$ of 4.7 ± 1.6 s and a diffusion coefficient of 0.061 ± 0.024 $\mu m^2 s^{-1}$ (Figures 2B and 2C). These diffusion coefficients are comparable to that of stably overexpressed DLL1 in CHO-K1 cells[41] and to those of other freely diffusing membrane proteins.[42]

We next determined the mobility of Notch and DLL4 molecules at the synapse by bleaching the fluorophore of interest 5–10 min after the onset of synapse formation. We monitored the fluorescence intensity of the non-bleached component within the ROI to delineate the synapse's location and ascertain its structural integrity throughout the 60-s observation period (Figures 2D, 2F, and 2H). In contrast to the rapid fluorescence recovery of N2-N, N2-C, or DLL4 in the surrounding cell surface membrane, NOTCH2 or DLL4 did not readily exchange when in synapses (10%–20% recovery after 60 s) (Figures 2E, 2G, and 2I). Thus, at the site of contact, both receptor and ligand exhibited greatly reduced exchange within the synapse and/or with the surrounding membrane.

Notch transendocytosis into the sender cell occurs after synapse formation

Transendocytosis of NECD and full-length Notch into ligand cells has been observed in cultured cells[23,26] and in flies.[26,43] Here, we monitored transendocytosis of NOTCH2 into DMS53 cells treated with blocking antibodies to DLL1, JAG1, and JAG2 as above. NOTCH2 accumulated into puncta within DMS53 (DLL4) cells only after synapse formation between paired cells (Figures 3A and 3B; Video S3). We quantified the relative amounts and stoichiometry of the N2-N (i.e., NECD) and N2-C tags to the DLL4 tag in these puncta by determining the fluorescence intensity ratios of different fluorophore pairs in these structures. Consistent with the observed 1:1 stoichiometric ratio of receptor to ligand in synapses, the N2-N (i.e., NECD) to DLL4 ratio, analyzed 60 min after synapse formation, was near 1:1 (Figure 3C; left, n = 174 puncta, ratio 0.6 ± 0.3). Analysis of the N2-N to DLL4 ratio in transendocytic puncta using the LLSM at an earlier timepoint, 30 min after pairing, gave a N2-N to DLL4 stoichiometric ratio of 0.9 ± 0.4, statistically indistinguishable from 1:1 (Figure S5A, related to Figure 3). The fractionally lower ratio of N2-N to DLL4 seen in puncta at the 60 min time point may have resulted from fusion of puncta containing both NOTCH2 and DLL4 with DLL4-only vesicles, which were also present, or from entry of a small fraction of the protein into a lower pH compartment where mNeonGreen fluorescence is attenuated.[44] In 54 of the puncta, only N2-N (i.e., NECD) and DLL4 were detected (Figure 3C, middle), whereas in the other puncta some N2-C was present along with N2-N and DLL4 (Figure 3C, right), indicative of occasional transendocytosis of full-length NOTCH2 as well as just the NECD. Quantification of the N2-N/N2-C ratio in these puncta showed an average value of 4:1, with considerable variation among the puncta.

While the majority of transendocytosis events involved only or predominantly N2-N (i.e., NECD), the entry of some N2-C into ligand cells along with N2-N suggested that some non-productive transendocytosis of full-length receptors occurred. Consistent with this interpretation, we did not observe any evidence of Notch signaling activity when ligand (DMS53) cells were probed using a luciferase reporter for a NICD-dependent response (Figures S5B and S5C, related to Figure 3), and we did not observe any accumulation of NICD in the nuclei of those cells. We also did not detect entry of DLL4 into the SVG-A (NOTCH2) receiver cells.

Occasionally, we were able to observe vesicle-like structures containing both ligand and receptor adjacent to synapse sites (Figure 3D). While our analyses did not allow us to determine unambiguously whether these vesicles originated directly from synapses or if the NOTCH2 and DLL4 instead accumulated in vesicles residing close to the contact site, it is possible these objects are vesicles captured at a very early stage shortly after initiation of transendocytosis.

Quantification of nuclear entry of NICD after cell contact

NICD can access the nucleus within 30 min of GSI removal[32] and can induce a transcriptional response in the nucleus within 60 min of Notch activation.[45,46] To quantify the amount of N2-C entering nuclei after cell-cell contact, we paired and imaged sender and receiver cells immediately (1–5 min) and 60 min after cell contact. Visual inspection of the nuclear region showed an increase of the fluorescent signal of N2-C, consistent with NICD nuclear entry (Figure 4A). The nuclear N2-C (i.e., NICD) concentration, calculated using a calibration curve with purified, recombinant HaloTag protein in solution labeled with JFX549 (Figures S5D and S5E, related to Figure 4), rose from 0.67 ± 0.5 nM before or immediately after cell contact to 2.1 ± 1.1 nM (equivalent to ~1,000–2,000 NICD molecules) at a time point 60 min after synapse formation (Figures 4B and 4C). The presence of intracellular puncta in the isolated NOTCH2 cells did not allow us to unambiguously follow the path of N2-C (i.e., NICD) from the synapse to the nucleus.

Temporal linkage between Notch processing and nuclear entry in living cells

We next established a quantitative spatiotemporal link among synapse formation, NECD transendocytosis, and NICD nuclear accumulation by using our microfluidic device to obtain imaging data of nine cell pairing events with a LLSM over a 60-min time course (Figure 5; Figures S6A–S6C, related to Figure 5; Videos S4 and S5). This approach enabled three-dimensional (3D) visualization with little photobleaching and phototoxicity compared with conventional spinning disk microscopes, thereby allowing repeated quantitative imaging of fluorescently tagged proteins expressed at endogenous levels over a prolonged period of time. The signal distribution of NOTCH2 at the cell surface was homogeneous in the absence of contact with DMS53 sender cells (t = 0), as assessed by analysis of N2-N and N2-C tag fluorescence, and the nuclear N2-C signal was minimal (Figures 5A and 5B). Again, Notch synapses rapidly formed at the site of contact between sender and receiver cells; NOTCH2 and DLL4 molecules accumulated within seconds after contact and the average synapse grew (assessed by the N2-N signal) from roughly 500 NOTCH2 molecules after 5 min of contact to a peak of roughly 2,000 molecules at 15–20 min. After 30 min, the synapses typically resolved (Figure 5; Figures S6A–S6C, related to Figure 5; Videos S4 and S5). The number of N2-N (i.e., NECD) molecules in puncta of DMS53 sender cells increased to a maximum at roughly 15 min before slowly decaying after 40 min, perhaps due to protein degradation, entry into a compartment with a lower pH, or both (Figure 5). Finally, the concentration of N2-C (i.e., NICD) in the nuclei of the receiver cells increased to a maximum of 1.4 ± 0.4 nM,

Please cite this article in press as: Tveriakhina et al., Temporal dynamics and stoichiometry in human Notch signaling from Notch synaptic complex formation to nuclear entry of the Notch intracellular domain, Developmental Cell (2024), https://doi.org/10.1016/j.devcel.2024.03.021

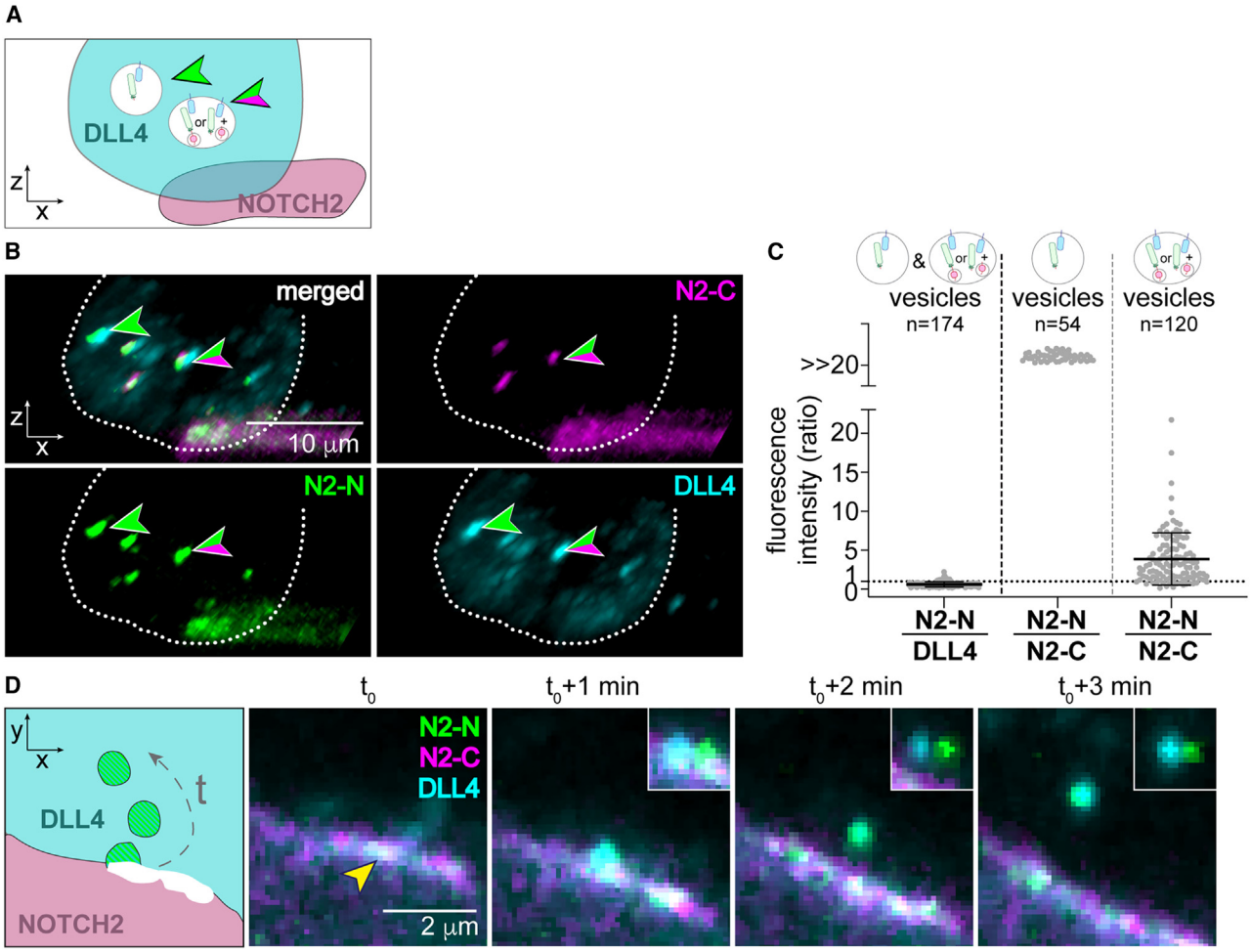

Figure 3. Transendocytosis of NOTCH2 into DLL4 cells takes place after synapse formation

(A) Schematic illustrating different compositions of NOTCH2-DLL4 complexes within DLL4 cell vesicles after cell pairing. Vesicles containing N2-N:DLL4 complexes (green arrowhead) and full-length NOTCH2:DLL4 complexes (containing both N2-N and N2-C; green/magenta arrowhead) are shown.

(B) Lattice light-sheet images of a DLL4 sender cell paired with a NOTCH2 receiver cell 20 min after contact. N2-N in green, N2-C in magenta, and DLL4 in cyan. Green arrowhead: vesicle containing only DLL4 and N2-N fluorescence. Green/magenta arrowhead: vesicle containing DLL4, N2-N, and N2-C fluorescence. Scale bars, 10 μm.

(C) Stoichiometric ratio of N2-N to DLL4 in vesicles (left), and of N2-N/N2-C in vesicles (center and right). The stoichiometric ratio for N2-N/N2-C in vesicles where N2-C was not detectable was arbitrarily set to >>20. Dotted line indicates the ratio of one observed in membrane and synapses (see Figure 1). n, number of vesicles analyzed (ROI). Error bars represent mean ± standard deviation.

(D) Schematic (left) and real-time lattice light-sheet microscopy images from a synapse at t_0 and subsequent 1 min intervals showing movement of N2-N and DLL4 fluorescence from the synapse into the sender cell over time. Synapse at t_0: yellow arrowhead. N2-N is shown in green, N2-C in magenta, and DLL4 in cyan. Insets show the three channels with a 5-pixel offset of the cyan channel for better visualization. Scale bars, 2 μm.

See also Figure S5.

corresponding to 1,000–2,000 molecules ~45 min after cell-cell contact, and remained steady until the end of the 60 min time course (Figure 5; Videos S4 and S5).

MIB1, ADAM10, and γ-secretase are not essential for synapse formation but are required for nuclear entry of NICD

The E3 ubiquitin ligase MIB1 is required in sender cells for ligand activity and subsequent receptor activation.[17] We eliminated *MIB1* in DLL4-HaloTag cells (*MIB1ko*) using CRISPR-Cas9 (Figures S6D and S6E, related to Figure 6) and paired these cells with our tagged SVG-A cells to monitor synapse formation, Notch transendocytosis, and N2-C accumulation in the nuclei of Notch cells. *MIB1ko* cells formed synapses efficiently but these synapses did not resolve after 60 min (Figure 6A). *MIB1ko* cells were also unable to induce transendocytosis of N2-N (i.e., NECD) (Figure 6B) and failed to produce a substantial increase in nuclear N2-C (i.e., NICD) within receiver cells (Figures 6C and 6D). These data show that MIB1 in sender cells is essential for synapse dissolution and confirm that it is required both for endocytosis of ligand-NECD complexes into the sender cell and for nuclear entry of NICD in the receiver cell.

We used protease inhibitors to investigate how preventing ADAM10 or γ-secretase cleavage of Notch affects the behavior

Please cite this article in press as: Tveriakhina et al., Temporal dynamics and stoichiometry in human Notch signaling from Notch synaptic complex formation to nuclear entry of the Notch intracellular domain, Developmental Cell (2024), https://doi.org/10.1016/j.devcel.2024.03.021

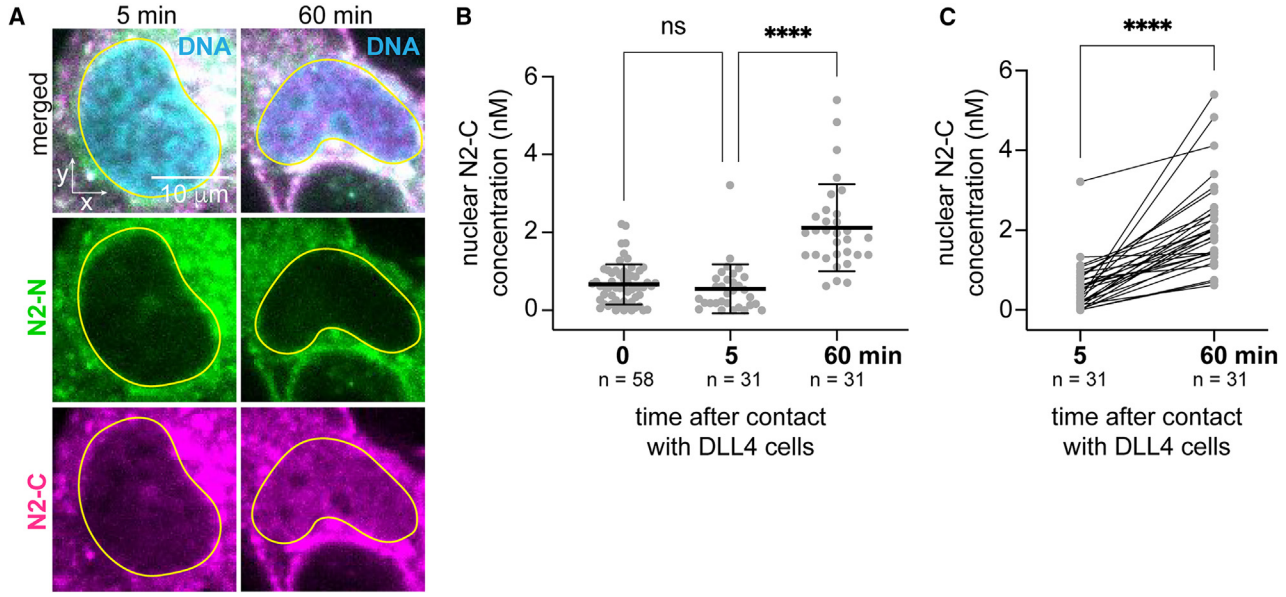

Figure 4. NICD nuclear entry after cell-cell contact

(A) Representative spinning disk confocal images of a NOTCH2 cell nucleus at 5 and at 60 min after contact with a DLL4 cell. Images show the maximum intensity projection of five planes through the center of the nucleus. N2-N is green, the N2-C tag (inclusive of NTM, NEXT, and NICD species) is magenta, and the cell nucleus/DNA is cyan (SiR-DNA). Nuclei are outlined with yellow lines. Scale bars, 10 μm.

(B and C) Quantitative analysis of the nuclear N2-C concentration (nM) before sender cell contact (0 min), and at 5 and 60 min after contact. Data are shown as a scatter plot in (B), and lines are drawn to connect paired concentration measurements at 5 and 60 min for each nucleus analyzed in (C). Error bars in (B) represent mean ± standard deviation. Statistical analysis was performed using Kruskal-Wallis one-way ANOVA (B) and Wilcoxon matched-pairs signed rank test (C). ****$p < 0.0001$; ns, not significant; n, number of analyzed nuclei.

See also Figure S5.

of DLL4 and NOTCH2 after cell pairing. While synapses still rapidly formed after contact, they resolved when cleavage at S2 was prevented with the metalloprotease inhibitor GI254023X (Figure S6F, related to Figure 6). This resolution may be due in part to transendocytosis of intact NOTCH2 into the sender cells because the ratio of signals from the N2-N and N2-C labels was 1:1 in the internalized structures (Figure 6E), indicating that ADAM10 inhibition did not interfere with the transendocytosis of full-length receptors. As expected, accumulation of N2-C (i.e., NICD) in receiver cell nuclei was greatly reduced (Figures 6F and 6G). Sender and receiver cell pairs also formed Notch synapses that resolved within 60 min in the presence of a GSI (compound E) (Figure S6F, related to Figure 6). Under these conditions, transendocytosis of N2-N (i.e., NECD) and full-length NOTCH2 into sender cells was not affected when compared with untreated cells (Figure 6E), indicating that release of the NECD by metalloprotease cleavage was still occurring. As expected, we failed to observe any increase in the nuclear content of N2-C (i.e., NICD) even 60 min after initiation of cell-cell contact (Figures 6F and 6G); these observations confirmed that γ-secretase was required for the cleavage step that produces NICD and for its subsequent entry into the nucleus.

DISCUSSION

In this work, we directly visualized NOTCH2 and DLL4 proteins from the onset of contact between DLL4 sender and NOTCH2 receiver cells until nuclear NICD in the receiver cells accumulated to steady state. A critical feature of this study was the use of genome-edited cells to ensure that the fluorescently tagged proteins were present at their natural abundance. Using quantitative fluorescence microscopy, we uncovered the appearance of a transient structure at the contact site between DLL4 sender and NOTCH2 receiver cells, here termed a Notch synapse. The Notch in the synapse is the source of the NICD that accumulates in the nucleus of the receiver cell.

Notch synapses form immediately after signal-sending and signal-receiving cells meet, as previously observed at contact sites in other model systems that used ectopic protein overexpression.[21,23–25,47] In contrast to our work, which uncovered the transient presence of a Notch synapse elicited immediately after sender-receiver cell contact, the previous studies using overexpressed proteins instead observed stable synapses that could last 24 h or longer after their formation.[21,25,47]

Strikingly, NOTCH2-DLL4 synapses accumulated normally but failed to resolve in synapses created between Notch receiver and sender cells lacking the E3 ligase MIB1. Because NECD (represented by the N2-N tag) from SVG-A sender cells failed to transendocytose into DMS53 (DLL4) *MIB1ko* cells, we disfavor a previous model for activation in which the furin-processed extracellular and transmembrane subunits of Notch are mechanically induced to dissociate at site S1 prior to metalloprotease cleavage.[23,48] Additionally, a model in which mechanical force supplied by bound ligand induces subunit dissociation at site S1 also predicts that ADAM10 inhibition would still be permissive of transendocytosis of liberated NECD into the sender cells, yet we observed that—although treatment with an ADAM10 inhibitor allowed transendocytosis of full-length NOTCH2 into the sender cells—it failed to permit transendocytosis of the free NECD. Our data are instead

Please cite this article in press as: Tveriakhina et al., Temporal dynamics and stoichiometry in human Notch signaling from Notch synaptic complex formation to nuclear entry of the Notch intracellular domain, Developmental Cell (2024), https://doi.org/10.1016/j.devcel.2024.03.021

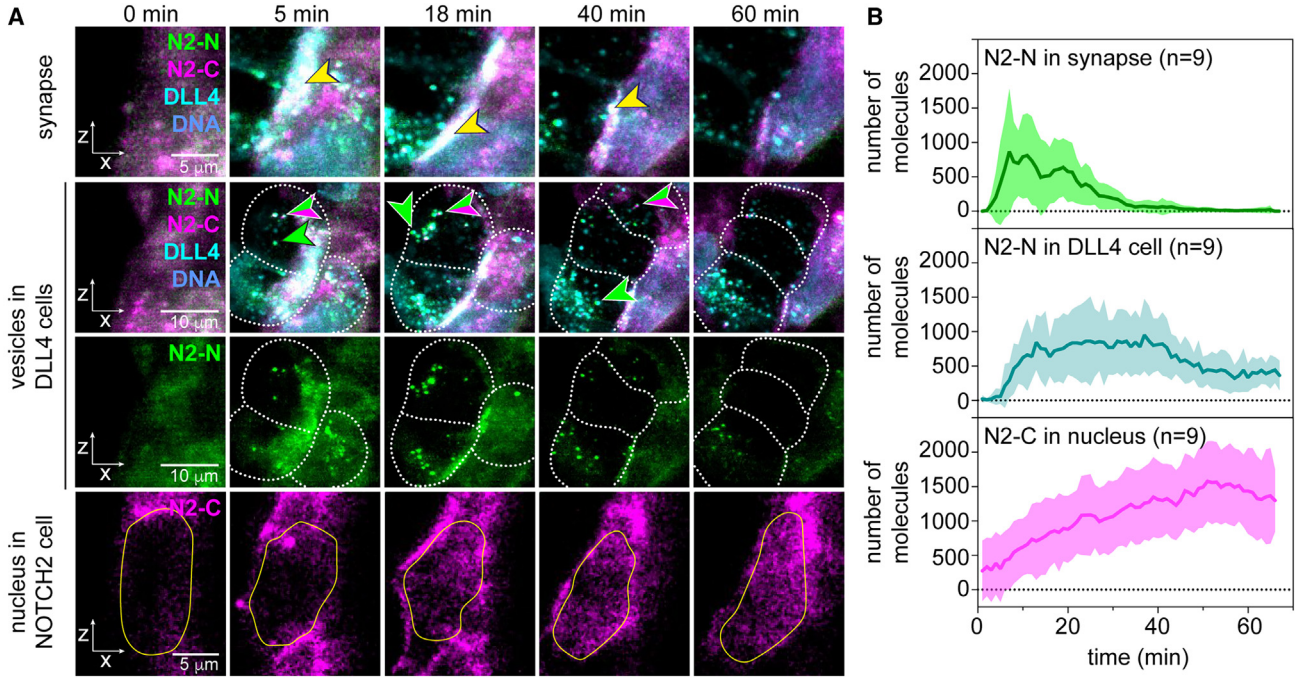

Figure 5. Real-time visualization of events after cell pairing

(A) Representative lattice light-sheet images from a time course observing a NOTCH2 cell before (0 min) and after contact with DLL4 cells (5–60 min). Panels highlight the formation and dissipation of synapses (top), the appearance of N2-N and N2-C positive vesicles in DLL4 cells (middle two rows) and the increase of N2-C associated signal in the nucleus of the NOTCH2 cell (bottom row). DLL4 cells are depicted by dotted lines (middle two rows) and the nucleus of the NOTCH2 cell, segmented using SiR-DNA labeling, is outlined with a yellow line (bottom row). N2-N is in green, the N2-C tag (NTM, NEXT, and/or NICD) is in magenta, and DLL4 in cyan. DNA was labeled using SiR-DNA and pseudocolored blue. Scale bars, 5 μm (top and bottom) and 10 μm (middle rows).

(B) Plots showing the calculated number of N2-N molecules in synapses (top), in DLL4-cell vesicles (middle) and the calculated number of N2-C molecules in nuclei of NOTCH2 cells (bottom) as a function of time after DLL4-cell contact. Graphs show mean ± standard deviation from n = 9 independent cell pairing events. See also Figure S6.

consistent with models positing that MIB1-dependent endocytosis of ligand is needed to induce ADAM10 cleavage of Notch at S2 in receiver cells, thereby liberating NECD. Our results are also consistent with findings in flies, in which replacement of the Notch negative regulatory region (NRR), which contains the S1 and S2 cut sites, by a domain more resistant to force-induced unfolding also leads to transendocytosis of full-length receptors, but not free NECD, into sender cells.[43] Unlike the studies in flies, however, in which ligands could enter the cells expressing the unfolding-resistant chimeric receptors, we did not observe entry of any DLL4 into the SVG-A receiver NOTCH2 cells when ADAM10 cleavage was chemically inhibited.

We showed that both NOTCH2 and DLL4 were mobile when on the cell surface but became fixed at the contact site once synapses formed. The mobility of DLL4 and NOTCH2 outside sites of contact resembled that predicted for their lateral diffusion in the membrane and was similar to that of overexpressed DLL1 in the membranes of CHO-K1 cells.[41]

There are at least two potential, non-exclusive mechanisms by which synapses could enhance signaling. First, synapses would increase the effective concentration of DLL4 and NOTCH2 in the synapse, favoring the bound state. Second, avidity effects from the presence of multiple ligand-receptor pairs would facilitate the ability of bound ligands to "pull" on Notch without dissociating, overcoming the modest monovalent affinity for single receptor-ligand pairs, notwithstanding the capacity of Notch-ligand complexes to form catch bonds.[49] Indeed, the relative immobility of the molecules in synapses suggests the existence of avidity effects that hold the molecules in place at the observed 1:1 stoichiometry (Figure 1).

Whether the stabilization of molecules in the synapses is a consequence of structured polymerization or another mechanism of self-association among the NOTCH2 and DLL4 molecules is not clear. There is evidence for weak self-association of the ankyrin domains of *Drosophila* Notch[50] and human NOTCH1, which contribute to the cooperative formation of dimeric transcription complexes on paired site DNA.[51] It is also true that the NRRs from NOTCH1, NOTCH2, and NOTCH3 share a crystal packing interface, the disruption of which induces signaling independent of ligand-receptor interaction.[52–54] However, the surface density of NOTCH2 and DLL4 in synapses appears to have been too low for them to be the only proteins present in synaptic sites, suggesting that additional proteins are needed to form the scaffold that holds them in a synapse.

NICD accumulation could be observed in the nucleus of receiver cells as early as 10 min after contact and plateaued after roughly 45 min. Live imaging of GFP-tagged Notch in sensory organ precursor cells of flies has shown that Notch can be seen in the nucleus on the pIIa cell as early as 10 min after cell division of the pIIa/pIIb precursor.[55] The accumulation of steady-state levels of NICD in the nucleus by ~45 min is also in agreement with the observed timing for transcriptional induction of Notch

Please cite this article in press as: Tveriakhina et al., Temporal dynamics and stoichiometry in human Notch signaling from Notch synaptic complex formation to nuclear entry of the Notch intracellular domain, Developmental Cell (2024), https://doi.org/10.1016/j.devcel.2024.03.021

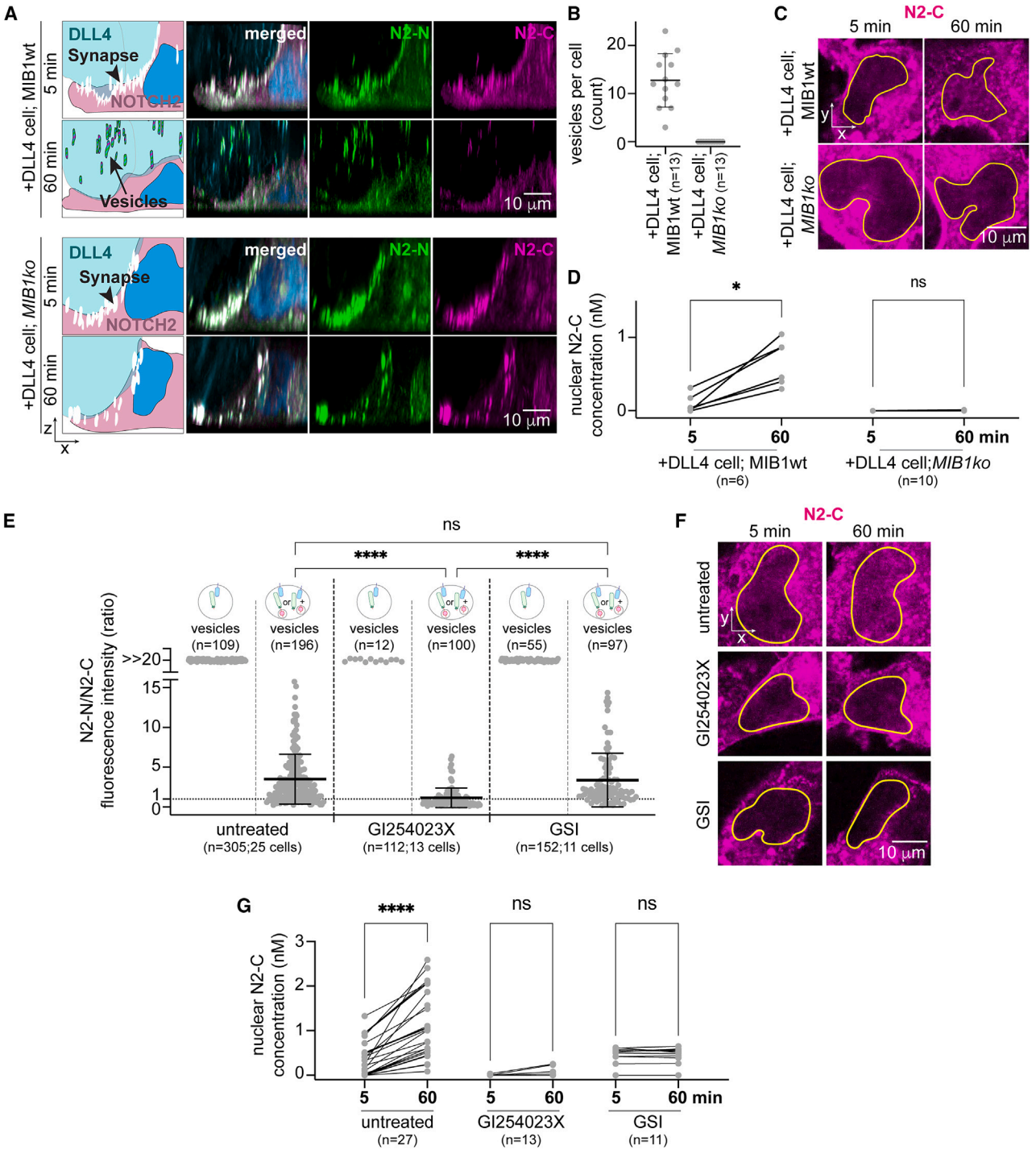

Figure 6. Effects of chemical and genetic perturbations on synapse formation, transendocytosis, and nuclear NICD entry

(A–D) Effects of knocking out MIB1 (*MIB1ko*) in sender cells. (A) Pairing of parental (top) and *MIB1ko* (bottom) DLL4 sender cells with NOTCH2 receiver cells, imaged using a spinning disk confocal microscope. Schematics (left) show cells, synapses (white, indicated by the black arrowhead), vesicles in DLL4 cells (black arrow), and nuclei (blue) of NOTCH2 cells. Images (right) show paired cells 5 and 60 min after contact. N2-N is shown in green, N2-C in magenta, DLL4 in cyan, and the nucleus of the NOTCH2 cell is pseudocolored blue. Images show the maximal intensity projection of a 3D z-stack of 14.84 μm. Scale bars, 10 μm. (B) Vesicles per DLL4 cell (MIB1 parental or *MIB1ko*) 60 min after NOTCH2 cell contact, assessed by manual counting. n, number of cells analyzed. (C) Representative images of nuclei from NOTCH2 cells co-cultured with parental or *MIB1ko* DLL4 sender cells, shown 5 and 60 min after direct contact. N2-C is shown in magenta. The images show the maximum intensity projection of five planes through the center of the nucleus. Yellow outlines denote nuclei as segmented using SiR-DNA labeling. Scale bars, 10 μm. (D) Quantitative analysis of the N2-C concentration (nM) in nuclei from NOTCH2 cells co-cultured with parental or *MIB1ko* DLL4 sender cells at 5 and 60 min after direct contact. n, number of nuclei analyzed.

(legend continued on next page)

Please cite this article in press as: Tveriakhina et al., Temporal dynamics and stoichiometry in human Notch signaling from Notch synaptic complex formation to nuclear entry of the Notch intracellular domain, Developmental Cell (2024), https://doi.org/10.1016/j.devcel.2024.03.021

target genes in *Drosophila* and cell culture systems.[45,56,57] The timing of these dynamics is also similar to that obtained by following the kinetics of proximity labeling of nuclear proteins associated with the Notch transcriptional response, which become labeled within 30–45 min of release from GSI inhibition.[32]

NICD entry into the nucleus of the receiver cell only occurred after synapse formation and only when NECD entry into the sender cell was also observed. The relatively uniform nuclear distribution of NICD, outside of nucleoli, from which it appeared to be excluded, made it possible to estimate the number and concentration of NICD molecules in the nucleus. Because the distribution of NICD in the receiver cell nuclei was not punctate, it appears that NICD does not accumulate in transcriptional hubs or nuclear foci, and that their formation are thus not required for a transcriptional response to NICD, at least in the first hour after cell contact.

More broadly, our studies illustrate the power of real-time imaging associated with signaling dynamics using proteins labeled at natural abundance. Using this approach, we uncovered dynamic formation and dissolution of synapses at sites of cell contact, quantified the stoichiometry of ligand-receptor complexes in synapses, and saw directly that synapse formation preceded transendocytosis of NECD into the sender cell, followed by entry of NICD into the receiver cell nucleus. Application of this strategy to other signaling systems should deepen understanding of their dynamics and molecular mechanisms with potential to make important contributions in the analysis of complex biological systems during cell differentiation *in vitro* and *in vivo*.

Limitations of the study

One limitation of this study is that it relies on a microfluidic system to initiate cell pairing. This mode of contact between Notch and ligand cells approximates events that occur between circulating and stromal cells, but it may not be representative of signaling events that take place in the context of intact tissues such as epithelia. Another limitation is that there are not enough data in the nine cell pairs we have analyzed to determine whether there is a correlation between synapse size and nuclear NICD. Though there may be a trend toward more nuclear NICD accumulating with increased synapse size (Figure S6, related to Figure 6), the statistical power to address this question definitively would require the acquisition of a large amount of additional data. Similarly, determination of the half-life of nuclear NICD would require an imaging period of several hours, a much longer duration than is technically feasible using the current system. Additional work will be needed to determine whether the dynamics of Notch and its ligands at sites of cell contact, including the formation and dissolution of synapses, is a general phenomenon, or is restricted to events that take place between circulating and stationary cell types.

STAR★METHODS

Detailed methods are provided in the online version of this paper and include the following:

- KEY RESOURCES TABLE
- RESOURCE AVAILABILITY
  - Lead contact
  - Materials availability
  - Data and code availability
- EXPERIMENTAL MODEL AND STUDY PARTICIPANT DETAILS
  - Cell culture
- METHOD DETAILS
  - Genome editing
  - JAGGED1-Fc expression and purification
  - RNA-seq sample preparation
  - RNA-seq library construction
  - RNA-seq analysis
  - Western blotting
  - Flow cytometry
  - Luciferase Notch reporter assay
  - Calibration of HaloTag^{JFX549} in solution
  - HaloTag and DNA labeling
  - Cell delivery and cell pairing in SD microscopy
  - Microfluidics device
  - Spinning disk (SD) confocal microscopy
  - LLSM modified with adaptive optics (MOSAIC)
  - Cell delivery and pairing for imaging in MOSAIC
  - Fluorescence recovery after photobleaching
- QUANTIFICATION AND STATISTICAL ANALYSIS
  - Ratiometric analysis
  - FRAP analysis
  - Nuclear N2-C (i.e., NICD) concentration
  - Quantification of 3D time-lapse imaged in MOSAIC
  - Statistical analysis

SUPPLEMENTAL INFORMATION

Supplemental information can be found online at https://doi.org/10.1016/j.devcel.2024.03.021.

ACKNOWLEDGMENTS

We thank members of the Blacklow and Kirchhausen laboratories, Matthieu Delincé for design of PDMS chips, Luke D. Lavis and Jonathan B. Grimm for the JF dyes, and the Center for Nanoscale Systems at Harvard University. This work was supported by NIH awards 1R35CA220340 (to S.C.B.), 1R01CA272484 (to S.C.B. and T.K.), 5R35GM130386 (to T.K.), and K99GM144750 (to J.M.R.); a Dean's Innovation Award (to S.C.B. and T.K.); a DFG Walter-Benjamin fellowship (TV-11/1 to L.T.); and the Ludwig Center at Harvard (to J.C.A.).

(E) N2-N/N2-C stoichiometric ratios in DLL4-containing vesicles of sender cells co-cultured with untreated, GI254023X-treated, or GSI-treated NOTCH2 cells. n, number of vesicles (ROI) analyzed.
(F) Representative images of nuclei from untreated, GI254023X-treated, or GSI-treated NOTCH2 cells at 5 and 60 min after direct contact with DLL4 cells. N2-C is shown in magenta. Yellow outlines denote nuclei as segmented using SiR-DNA labeling. Each image shows the maximum intensity projection of three planes through the center of the nucleus. Scale bars, 10 μm.
(G) Quantitative analysis of the N2-C concentration (nM) in nuclei of untreated, GI254023X-treated or GSI-treated NOTCH2 cells at 5 and 60 min after contact with sender cells. N, number of nuclei analyzed. Error bars in (B) and (E) show mean ± standard deviation. Statistical analyses in were performed using the Wilcoxon matched-pairs signed rank test (D and G), and Kruskal-Wallis one-way ANOVA (E). Dotted line in (E) indicates a ratio of one. *$p < 0.05$, ****$p < 0.0001$; ns, not significant.
See also Figure S6.

AUTHOR CONTRIBUTIONS

L.T., G.S., T.K., and S.C.B. conceived the project. S.C.B. and T.K. acquired funding. L.T., G.S., E.D.E., and R.B.D.C.C. performed experiments. L.T. and G.S. analyzed the data. E.D.E. and J.M.R. processed and analyzed RNA-seq data. A.P.M. generated A673 *JAG1ko* cells. J.S.Y. helped with the fabrication of microfluidic chips. A.P.M. and J.C.A. assisted with data analysis and interpretation. L.T., G.S., T.K., and S.C.B. wrote the manuscript with input from all authors. All authors provided feedback and agreed on the final manuscript.

DECLARATION OF INTERESTS

S.C.B. is on the board for the Institute for Protein Innovation and the Revson Foundation, on the SAB for MPM Capital and Erasca, and consults for Scorpion Therapeutics and Odyssey Therapeutics- on unrelated projects. T.K. is a member of the Medical Advisory Board of AI Therapeutics. J.C.A. is a consultant for Ayala Pharmaceuticals, Cellestia, SpringWorks, and Remix Therapeutics.

Received: October 5, 2023
Revised: January 10, 2024
Accepted: March 11, 2024
Published: April 3, 2024

REFERENCES

1. Bray, S.J. (2016). Notch signalling in context. Nat. Rev. Mol. Cell Biol. *17*, 722–735. https://doi.org/10.1038/nrm.2016.94.
2. Kovall, R.A., Gebelein, B., Sprinzak, D., and Kopan, R. (2017). The Canonical Notch Signaling Pathway: Structural and Biochemical Insights into Shape, Sugar, and Force. Dev. Cell *41*, 228–241. https://doi.org/10.1016/j.devcel.2017.04.001.
3. Sprinzak, D., and Blacklow, S.C. (2021). Biophysics of Notch Signaling. Annu. Rev. Biophys. *50*, 157–189. https://doi.org/10.1146/annurev-biophys-101920-082204.
4. Kamath, B.M., Bauer, R.C., Loomes, K.M., Chao, G., Gerfen, J., Hutchinson, A., Hardikar, W., Hirschfield, G., Jara, P., Krantz, I.D., et al. (2012). NOTCH2 mutations in Alagille syndrome. J. Med. Genet. *49*, 138–144. https://doi.org/10.1136/jmedgenet-2011-100544.
5. Li, L., Krantz, I.D., Deng, Y., Genin, A., Banta, A.B., Collins, C.C., Qi, M., Trask, B.J., Kuo, W.L., Cochran, J., et al. (1997). Alagille syndrome is caused by mutations in human Jagged1, which encodes a ligand for Notch1. Nat. Genet. *16*, 243–251. https://doi.org/10.1038/ng0797-243.
6. Oda, T., Elkahloun, A.G., Pike, B.L., Okajima, K., Krantz, I.D., Genin, A., Piccoli, D.A., Meltzer, P.S., Spinner, N.B., Collins, F.S., and Chandrasekharappa, S.C. (1997). Mutations in the human Jagged1 gene are responsible for Alagille syndrome. Nat. Genet. *16*, 235–242. https://doi.org/10.1038/ng0797-235.
7. Joutel, A., Corpechot, C., Ducros, A., Vahedi, K., Chabriat, H., Mouton, P., Alamowitch, S., Domenga, V., Cécillion, M., Marechal, E., et al. (1996). Notch3 mutations in CADASIL, a hereditary adult-onset condition causing stroke and dementia. Nature *383*, 707–710. https://doi.org/10.1038/383707a0.
8. Weng, A.P., Ferrando, A.A., Lee, W., Morris, J.P., 4th, Silverman, L.B., Sanchez-Irizarry, C., Blacklow, S.C., Look, A.T., and Aster, J.C. (2004). Activating mutations of NOTCH1 in human T cell acute lymphoblastic leukemia. Science *306*, 269–271. https://doi.org/10.1126/science.1102160.
9. Puente, X.S., Pinyol, M., Quesada, V., Conde, L., Ordóñez, G.R., Villamor, N., Escaramis, G., Jares, P., Beà, S., González-Díaz, M., et al. (2011). Whole-genome sequencing identifies recurrent mutations in chronic lymphocytic leukaemia. Nature *475*, 101–105. https://doi.org/10.1038/nature10113.
10. Aster, J.C., Pear, W.S., and Blacklow, S.C. (2017). The varied roles of Notch in cancer. Annu. Rev. Pathol. *12*, 245–275. https://doi.org/10.1146/annurev-pathol-052016-100127.
11. Agrawal, N., Frederick, M.J., Pickering, C.R., Bettegowda, C., Chang, K., Li, R.J., Fakhry, C., Xie, T.-X., Zhang, J., Wang, J., et al. (2011). Exome sequencing of head and neck squamous cell carcinoma reveals inactivating mutations in NOTCH1. Science *333*, 1154–1157. https://doi.org/10.1126/science.1206923.
12. Wang, N.J., Sanborn, Z., Arnett, K.L., Bayston, L.J., Liao, W., Proby, C.M., Leigh, I.M., Collisson, E.A., Gordon, P.B., Jakkula, L., et al. (2011). Loss-of-function mutations in Notch receptors in cutaneous and lung squamous cell carcinoma. Proc. Natl. Acad. Sci. USA *108*, 17761–17766. https://doi.org/10.1073/pnas.1114669108.
13. Martincorena, I., Roshan, A., Gerstung, M., Ellis, P., Van Loo, P., McLaren, S., Wedge, D.C., Fullam, A., Alexandrov, L.B., Tubio, J.M., et al. (2015). Tumor evolution. High burden and pervasive positive selection of somatic mutations in normal human skin. Science *348*, 880–886. https://doi.org/10.1126/science.aaa6806.
14. Logeat, F., Bessia, C., Brou, C., LeBail, O., Jarriault, S., Seidah, N.G., and Israël, A. (1998). The Notch1 receptor is cleaved constitutively by a furin-like convertase. Proc. Natl. Acad. Sci. USA *95*, 8108–8112. https://doi.org/10.1073/pnas.95.14.8108.
15. Blaumueller, C.M., Qi, H., Zagouras, P., and Artavanis-Tsakonas, S. (1997). Intracellular cleavage of Notch leads to a heterodimeric receptor on the plasma membrane. Cell *90*, 281–291. https://doi.org/10.1016/s0092-8674(00)80336-0.
16. Daskalaki, A., Shalaby, N.A., Kux, K., Tsoumpekos, G., Tsibidis, G.D., Muskavitch, M.A.T., and Delidakis, C. (2011). Distinct intracellular motifs of Delta mediate its ubiquitylation and activation by Mindbomb1 and Neuralized. J. Cell Biol. *195*, 1017–1031. https://doi.org/10.1083/jcb.201105166.
17. Guo, B., McMillan, B.J., and Blacklow, S.C. (2016). Structure and function of the Mind bomb E3 ligase in the context of Notch signal transduction. Curr. Opin. Struct. Biol. *41*, 38–45. https://doi.org/10.1016/j.sbi.2016.05.012.
18. McMillan, B.J., Schnute, B., Ohlenhard, N., Zimmerman, B., Miles, L., Beglova, N., Klein, T., and Blacklow, S.C. (2015). A Tail of Two Sites: A Bipartite Mechanism for Recognition of Notch Ligands by Mind Bomb E3 Ligases. Mol. Cell *57*, 912–924. https://doi.org/10.1016/j.molcel.2015.01.019.
19. Okano, M., Matsuo, H., Nishimura, Y., Hozumi, K., Yoshioka, S., Tonoki, A., and Itoh, M. (2016). Mib1 modulates dynamin 2 recruitment via Snx18 to promote Dll1 endocytosis for efficient Notch signaling. Genes Cells *21*, 425–441. https://doi.org/10.1111/gtc.12350.
20. Artavanis-Tsakonas, S., Muskavitch, M.A.T., and Yedvobnick, B. (1983). Molecular cloning of Notch, a locus affecting neurogenesis in Drosophila melanogaster. Proc. Natl. Acad. Sci. USA *80*, 1977–1981. https://doi.org/10.1073/pnas.80.7.1977.
21. Fehon, R.G., Kooh, P.J., Rebay, I., Regan, C.L., Xu, T., Muskavitch, M.A., and Artavanis-Tsakonas, S. (1990). Molecular interactions between the protein products of the neurogenic loci Notch and Delta, two EGF-homologous genes in Drosophila. Cell *61*, 523–534. https://doi.org/10.1016/0092-8674(90)90534-l.
22. Klueg, K.M., and Muskavitch, M.A. (1999). Ligand-receptor interactions and trans-endocytosis of Delta, Serrate and Notch: members of the Notch signalling pathway in Drosophila. J. Cell Sci. *112*, 3289–3297. https://doi.org/10.1242/jcs.112.19.3289.
23. Nichols, J.T., Miyamoto, A., Olsen, S.L., D'Souza, B., Yao, C., and Weinmaster, G. (2007). DSL ligand endocytosis physically dissociates Notch1 heterodimers before activating proteolysis can occur. J. Cell Biol. *176*, 445–458. https://doi.org/10.1083/jcb.200609014.
24. Meloty-Kapella, L., Shergill, B., Kuon, J., Botvinick, E., and Weinmaster, G. (2012). Notch ligand endocytosis generates mechanical pulling force dependent on dynamin, epsins, and actin. Dev. Cell *22*, 1299–1312. https://doi.org/10.1016/j.devcel.2012.04.005.
25. Chapman, G., Major, J.A., Iyer, K., James, A.C., Pursglove, S.E., Moreau, J.L.M., and Dunwoodie, S.L. (2016). Notch1 endocytosis is induced by ligand and is required for signal transduction. Biochim. Biophys. Acta *1863*, 166–177. https://doi.org/10.1016/j.bbamcr.2015.10.021.

26. Parks, A.L., Klueg, K.M., Stout, J.R., and Muskavitch, M.A. (2000). Ligand endocytosis drives receptor dissociation and activation in the Notch pathway. Development *127*, 1373–1385. https://doi.org/10.1242/dev.127.7.1373.

27. Mumm, J.S., Schroeter, E.H., Saxena, M.T., Griesemer, A., Tian, X., Pan, D.J., Ray, W.J., and Kopan, R. (2000). A ligand-induced extracellular cleavage regulates gamma-secretase-like proteolytic activation of Notch1. Mol. Cell *5*, 197–206. https://doi.org/10.1016/S1097-2765(00)80416-5.

28. van Tetering, G., van Diest, P., Verlaan, I., van der Wall, E., Kopan, R., and Vooijs, M. (2009). Metalloprotease ADAM10 is required for Notch1 site 2 cleavage. J. Biol. Chem. *284*, 31018–31027. https://doi.org/10.1074/jbc.M109.006775.

29. Chapman, G., Sparrow, D.B., Kremmer, E., and Dunwoodie, S.L. (2011). Notch inhibition by the ligand DELTA-LIKE 3 defines the mechanism of abnormal vertebral segmentation in spondylocostal dysostosis. Hum. Mol. Genet. *20*, 905–916. https://doi.org/10.1093/hmg/ddq529.

30. Chen, B.-C., Legant, W.R., Wang, K., Shao, L., Milkie, D.E., Davidson, M.W., Janetopoulos, C., Wu, X.S., Hammerv, J.A., iii, Liu, Z., et al. (2014). Lattice Light Sheet Microscopy: Imaging Molecules to Embryos at High Spatiotemporal Resolution Bi-Chang. Science *346*, 1257998. https://doi.org/10.1126/science.1257998.Lattice.

31. Chou, Y.-Y., Krupp, A., Kaynor, C., Gaudin, R., Ma, M., Cahir-McFarland, E., and Kirchhausen, T. (2016). Inhibition of JCPyV infection mediated by targeted viral genome editing using CRISPR/Cas9. Sci. Rep. *6*, 36921. https://doi.org/10.1038/srep36921.

32. Martin, A.P., Bradshaw, G.A., Eisert, R.J., Egan, E.D., Tveriakhina, L., Rogers, J.M., Dates, A.N., Scanavachi, G., Aster, J.C., Kirchhausen, T., et al. (2023). A spatiotemporal Notch interaction map from plasma membrane to nucleus. Sci. Signal. *16*, eadg6474. https://doi.org/10.1126/scisignal.adg6474.

33. Kuleshov, M.V., Jones, M.R., Rouillard, A.D., Fernandez, N.F., Duan, Q., Wang, Z., Koplev, S., Jenkins, S.L., Jagodnik, K.M., Lachmann, A., et al. (2016). Enrichr: a comprehensive gene set enrichment analysis web server 2016 update. Nucleic Acids Res. *44*, W90–W97. https://doi.org/10.1093/nar/gkw377.

34. Chen, E.Y., Tan, C.M., Kou, Y., Duan, Q., Wang, Z., Meirelles, G.V., Clark, N.R., and Ma'ayan, A. (2013). Enrichr: interactive and collaborative HTML5 gene list enrichment analysis tool. BMC Bioinformatics *14*, 128. https://doi.org/10.1186/1471-2105-14-128.

35. Los, G.V., Encell, L.P., McDougall, M.G., Hartzell, D.D., Karassina, N., Zimprich, C., Wood, M.G., Learish, R., Ohana, R.F., Urh, M., et al. (2008). HaloTag: a novel protein labeling technology for cell imaging and protein analysis. ACS Chem. Biol. *3*, 373–382. https://doi.org/10.1021/cb800025k.

36. Shaner, N.C., Lambert, G.G., Chammas, A., Ni, Y., Cranfill, P.J., Baird, M.A., Sell, B.R., Allen, J.R., Day, R.N., Israelsson, M., et al. (2013). A bright monomeric green fluorescent protein derived from Branchiostoma lanceolatum. Nat. Methods *10*, 407–409. https://doi.org/10.1038/nmeth.2413.

37. Grimm, J.B., Xie, L., Casler, J.C., Patel, R., Tkachuk, A.N., Choi, H., Lippincott-Schwartz, J., Brown, T.A., Glick, B.S., Liu, Z., and Lavis, L.D. (2020). Deuteration improves small-molecule fluorophores. Preprint at bioRxiv. https://doi.org/10.1101/2020.08.17.250027.

38. Tran, I.T., Sandy, A.R., Carulli, A.J., Ebens, C., Chung, J., Shan, G.T., Radojcic, V., Friedman, A., Gridley, T., Shelton, A., et al. (2013). Blockade of individual Notch ligands and receptors controls graft-versus-host disease. J. Clin. Invest. *123*, 1590–1604. https://doi.org/10.1172/JCI65477.

39. Lafkas, D., Shelton, A., Chiu, C., de Leon Boenig, G., Chen, Y., Stawicki, S.S., Siltanen, C., Reichelt, M., Zhou, M., Wu, X., et al. (2015). Therapeutic antibodies reveal Notch control of transdifferentiation in the adult lung. Nature *528*, 127–131. https://doi.org/10.1038/nature15715.

40. Ridgway, J., Zhang, G., Wu, Y., Stawicki, S., Liang, W.-C., Chanthery, Y., Kowalski, J., Watts, R.J., Callahan, C., Kasman, I., et al. (2006). Inhibition of Dll4 signalling inhibits tumour growth by deregulating angiogenesis. Nature *444*, 1083–1087. https://doi.org/10.1038/nature05313.

41. Khait, I., Orsher, Y., Golan, O., Binshtok, U., Gordon-Bar, N., Amir-Zilberstein, L., and Sprinzak, D. (2016). Quantitative Analysis of Delta-like 1 Membrane Dynamics Elucidates the Role of Contact Geometry on Notch Signaling. Cell Rep. *14*, 225–233. https://doi.org/10.1016/j.celrep.2015.12.040.

42. Jacobson, K., Ishihara, A., and Inman, R. (1987). Lateral diffusion of proteins in membranes. Annu. Rev. Physiol. *49*, 163–175. https://doi.org/10.1146/annurev.ph.49.030187.001115.

43. Langridge, P.D., and Struhl, G. (2017). Epsin-Dependent Ligand Endocytosis Activates Notch by Force. Cell *171*, 1383–1396.e12. https://doi.org/10.1016/j.cell.2017.10.048.

44. Tutol, J.N., Kam, H.C., and Dodani, S.C. (2019). Identification of mNeonGreen as a pH-dependent, turn-on fluorescent protein sensor for chloride. ChemBioChem *20*, 1759–1765. https://doi.org/10.1002/cbic.201900147.

45. Ilagan, M.X.G., Lim, S., Fulbright, M., Piwnica-Worms, D., and Kopan, R. (2011). Real-time imaging of Notch activation with a luciferase complementation-based reporter. Sci. Signal. *4*, rs7. https://doi.org/10.1126/scisignal.2001656.

46. Falo-Sanjuan, J., and Bray, S. (2022). Notch-dependent and -independent transcription are modulated by tissue movements at gastrulation. Elife *11*, e73656. https://doi.org/10.7554/eLife.73656.

47. Khamaisi, B., Luca, V.C., Blacklow, S.C., and Sprinzak, D. (2022). Functional Comparison between Endogenous and Synthetic Notch Systems. ACS Synth. Biol. *11*, 3343–3353. https://doi.org/10.1021/acssynbio.2c00247.

48. Chastagner, P., Rubinstein, E., and Brou, C. (2017). Ligand-activated Notch undergoes DTX4-mediated ubiquitylation and bilateral endocytosis before ADAM10 processing. Sci. Signal. *10*, 1–14. https://doi.org/10.1126/scisignal.aag2989.

49. Luca, V.C., Kim, B.C., Ge, C., Kakuda, S., Wu, D., Roein-Peikar, M., Haltiwanger, R.S., Zhu, C., Ha, T., and Garcia, K.C. (2017). Notch-Jagged complex structure implicates a catch bond in tuning ligand sensitivity. Science *355*, 1320–1324. https://doi.org/10.1126/science.aaf9739.

50. Allgood, A.G., and Barrick, D. (2011). Mapping the Deltex-binding surface on the notch ankyrin domain using analytical ultracentrifugation. J. Mol. Biol. *414*, 243–259. https://doi.org/10.1016/j.jmb.2011.09.050.

51. Arnett, K.L., Hass, M., McArthur, D.G., Ilagan, M.X.G., Aster, J.C., Kopan, R., and Blacklow, S.C. (2010). Structural and mechanistic insights into cooperative assembly of dimeric Notch transcription complexes. Nat. Struct. Mol. Biol. *17*, 1312–1317. https://doi.org/10.1038/nsmb.1938.

52. Xu, X., Choi, S.H., Hu, T., Tiyanont, K., Habets, R., Groot, A.J., Vooijs, M., Aster, J.C., Chopra, R., Fryer, C., and Blacklow, S.C. (2015). Insights into Autoregulation of Notch3 from Structural and Functional Studies of Its Negative Regulatory Region. Structure *23*, 1227–1235. https://doi.org/10.1016/j.str.2015.05.001.

53. Gordon, W.R., Roy, M., Vardar-Ulu, D., Garfinkel, M., Mansour, M.R., Aster, J.C., and Blacklow, S.C. (2009). Structure of the Notch1-negative regulatory region: Implications for normal activation and pathogenic signaling in T-ALL. Blood *113*, 4381–4390. https://doi.org/10.1182/blood-2008-08-174748.

54. Gordon, W.R., Vardar-Ulu, D., Histen, G., Sanchez-Irizarry, C., Aster, J.C., and Blacklow, S.C. (2007). Structural basis for autoinhibition of Notch. Nat. Struct. Mol. Biol. *14*, 295–300. https://doi.org/10.1038/nsmb1227.

55. Couturier, L., Vodovar, N., and Schweisguth, F. (2012). Endocytosis by Numb breaks Notch symmetry at cytokinesis. Nat. Cell Biol. *14*, 131–139. https://doi.org/10.1038/ncb2419.

56. Pillidge, Z., and Bray, S.J. (2019). SWI/SNF chromatin remodeling controls Notch-responsive enhancer accessibility. EMBO Rep. *20*, e46944. https://doi.org/10.15252/embr.201846944.

57. Falo-Sanjuan, J., Lammers, N.C., Garcia, H.G., and Bray, S.J. (2019). Enhancer Priming Enables Fast and Sustained Transcriptional Responses to Notch Signaling. Dev. Cell *50*, 411–425.e8. https://doi.org/10.1016/j.devcel.2019.07.002.

58. Chou, Y.-Y., Upadhyayula, S., Houser, J., He, K., Skillern, W., Scanavachi, G., Dang, S., Sanyal, A., Ohashi, K.G., Di Caprio, G., et al. (2021). Inherited nuclear pore substructures template post-mitotic pore assembly. Dev. Cell *56*, 1786–1803.e9. https://doi.org/10.1016/j.devcel.2021.05.015.

59. Kurooka, H., Kuroda, K., and Honjo, T. (1998). Roles of the ankyrin repeats and C-terminal region of the mouse Notch1 intracellular region. Nucleic Acids Res. *26*, 5448–5455. https://doi.org/10.1093/nar/26.23.5448.

60. Minoguchi, S., Taniguchi, Y., Kato, H., Okazaki, T., Strobl, L.J., Zimber-Strobl, U., Bornkamm, G.W., and Honjo, T. (1997). RBP-L, a transcription factor related to RBP-Jkappa. Mol. Cell. Biol. *17*, 2679–2687. https://doi.org/10.1128/MCB.17.5.2679.

61. Wilhelm, J., Kühn, S., Tarnawski, M., Gotthard, G., Tünnermann, J., Tänzer, T., Karpenko, J., Mertes, N., Xue, L., Uhrig, U., et al. (2021). Kinetic and Structural Characterization of the Self-Labeling Protein Tags HaloTag7, SNAP-tag, and CLIP-tag. Biochemistry *60*, 2560–2575. https://doi.org/10.1021/acs.biochem.1c00258.

62. Aguet, F., Upadhyayula, S., Gaudin, R., Chou, Y.Y., Cocucci, E., He, K., Chen, B.C., Mosaliganti, K., Pasham, M., Skillern, W., et al. (2016). Membrane dynamics of dividing cells imaged by lattice light-sheet microscopy. Mol. Biol. Cell *27*, 3418–3435. https://doi.org/10.1091/mbc.E16-03-0164.

63. Aguet, F., Antonescu, C.N., Mettlen, M., Schmid, S.L., and Danuser, G. (2013). Advances in analysis of low signal-to-noise images link dynamin and AP2 to the functions of an endocytic checkpoint. Dev. Cell *26*, 279–291. https://doi.org/10.1016/j.devcel.2013.06.019.

64. Schindelin, J., Arganda-Carreras, I., Frise, E., Kaynig, V., Longair, M., Pietzsch, T., Preibisch, S., Rueden, C., Saalfeld, S., Schmid, B., et al. (2012). Fiji: an open-source platform for biological-image analysis. Nat. Methods *9*, 676–682. https://doi.org/10.1038/nmeth.2019.

65. Langmead, B., Trapnell, C., Pop, M., and Salzberg, S.L. (2009). Ultrafast and memory-efficient alignment of short DNA sequences to the human genome. Genome Biol. *10*, R25. https://doi.org/10.1186/gb-2009-10-3-r25.

66. Dobin, A., Davis, C.A., Schlesinger, F., Drenkow, J., Zaleski, C., Jha, S., Batut, P., Chaisson, M., and Gingeras, T.R. (2013). STAR: ultrafast universal RNA-seq aligner. Bioinformatics *29*, 15–21. https://doi.org/10.1093/bioinformatics/bts635.

67. Liao, Y., Smyth, G.K., and Shi, W. (2014). featureCounts: an efficient general purpose program for assigning sequence reads to genomic features. Bioinformatics *30*, 923–930. https://doi.org/10.1093/bioinformatics/btt656.

68. Love, M.I., Huber, W., and Anders, S. (2014). Moderated estimation of fold change and dispersion for RNA-seq data with DESeq2. Genome Biol. *15*, 550. https://doi.org/10.1186/s13059-014-0550-8.

69. Salman, M.M., Marsh, G., Kusters, I., Delincé, M., Di Caprio, G., Upadhyayula, S., de Nola, G., Hunt, R., Ohashi, K.G., Gray, T., et al. (2020). Design and Validation of a Human Brain Endothelial Microvessel-on-a-Chip Open Microfluidic Model Enabling Advanced Optical Imaging. Front. Bioeng. Biotechnol. *8*, 573775. https://doi.org/10.3389/fbioe.2020.573775.

70. Govindaraj, K., and Post, J.N. (2021). Using FRAP to Quantify Changes in Transcription Factor Dynamics After Cell Stimulation: Cell Culture, FRAP, Data Analysis, and Visualization. Methods Mol. Biol. *2221*, 109–139. https://doi.org/10.1007/978-1-0716-0989-7_9.

71. Kang, M., Day, C.A., Kenworthy, A.K., and DiBenedetto, E. (2012). Simplified equation to extract diffusion coefficients from confocal FRAP data. Traffic *13*, 1589–1600. https://doi.org/10.1111/tra.12008.

Please cite this article in press as: Tveriakhina et al., Temporal dynamics and stoichiometry in human Notch signaling from Notch synaptic complex formation to nuclear entry of the Notch intracellular domain, Developmental Cell (2024), https://doi.org/10.1016/j.devcel.2024.03.021

STAR★METHODS

KEY RESOURCES TABLE

REAGENT or RESOURCE	SOURCE	IDENTIFIER
Antibodies		
anti-Notch2	Cell Signaling Technology	Cat# 5732, RRID: AB_10693319
anti-JAG1	Santa Cruz Biotechnology	Cat# sc-8303, RRID: AB_649685
anti-DLL4	Cell Signaling Technology	Cat# 96406, RRID: AB_2800263
anti-MIB1 (N-terminal)	Abcam	Cat# ab124929, RRID: AB_11127834
anti-MIB1 (C-Terminal)	Sigma	Cat# M5948, RRID: AB_1841007
anti-Vinculin	Abcam	Cat# ab129002
anti-GAPDH	Cell Signaling Technology	Cat# 5174, RRID: AB_10622025
IRDye 800CW Donkey anti-Rabbit	LI-COR Biosciences	Cat# 926-32213, RRID: AB_621848
IRDye 680RD Goat anti-Mouse	LI-COR Biosciences	Cat#926-68070, RRID: AB_10956588
APC anti-human NOTCH2	BioLegend	Cat# 348305, RRID: AB_10662412
APC Mouse IgG2a, κ Isotype Ctrl (FC) Antibody	BioLegend	Cat# 400221, RRID: AB_2891178
PE anti-human JAG1	BD Biosciences	Cat# 565495, RRID: AB_2739264
PE Mouse IgG1, κ Isotype Control	BD Biosciences	Cat# 555749, RRID: AB_396091
PE anti-human JAG2	BioLegend	Cat# 346904, RRID: AB_2128374
PE Mouse IgG1, κ Isotype Ctrl Antibody	BioLegend	Cat# 400112, RRID: AB_2847829
DLL1 Antibody, anti-human, APC	Miltenyi Biotec	Cat# 130-096-961, RRID: AB_2651557
Isotype Control Antibody, mouse IgG1, APC	Miltenyi Biotec	Cat# 130-113-196, RRID: AB_2733440
APC anti-human DLL4	BioLegend	Cat# 346508, RRID: AB_11204071
APC Mouse IgG1, κ Isotype Ctrl Antibody	BioLegend	Cat# 400120, RRID: AB_2888687
anti-DLL1 (blocking)	Tran et al.[38]; Genentech	N/A
anti-DLL4 (blocking)	Ridgway et al.[40]; Genentech	N/A
anti-JAG1 (blocking)	Lafkas et al.,[39] Genentech	N/A
anti-JAG2 (blocking)	Lafkas et al.,[39] Genentech	N/A
Bacterial and virus strains		
BL21 DE3 pLysS	Thermo Fisher Scientific	Cat# C606010
Chemicals, peptides, and recombinant proteins		
FBS	GeminiBio	Cat# 100-106
Penicillin-Streptomycin	Thermo Fisher Scientific	Cat# 15140163
Trypsin/0.53 mM EDTA in HBSS	Corning	Cat# 25-051-CI
Gibco FluoroGrite DMEM	Thermo Fisher Scientific	Cat# A1896701
DMEM	Corning	Cat# 10-017-CV
FBS	Gibco	Cat# 10437028
EDTA 0.5 M	Thermo Fisher Scientific	Cat# 15-575-020
G418	Gibco	Cat# 10131035
Puromycin	InvivoGen	Cat# ant-pr-1
DPBS	Corning	Cat# 21-031-CV
Protein A agarose	Millipore	Cat# 16-125
Gibco HEPES	Gibco	Cat# 15630080
NaCl	VWR	Cat# 0241-10KG
HEPES	Sigma-Aldrich	Cat# H4034-1KG
GlutaMax	Thermo Fisher Scientific	Cat# 35050061
Glycerol	Americanbio	Cat# AB00751-04000
Trizma base	Sigma-Aldrich	Cat# T1503-5KG
Glycine	Sigma-Aldrich	Cat# G7126-5KG

(*Continued on next page*)

Please cite this article in press as: Tveriakhina et al., Temporal dynamics and stoichiometry in human Notch signaling from Notch synaptic complex formation to nuclear entry of the Notch intracellular domain, Developmental Cell (2024), https://doi.org/10.1016/j.devcel.2024.03.021

Continued

REAGENT or RESOURCE	SOURCE	IDENTIFIER
β−Mercaptoethanol	Sigma-Aldrich	Cat# M6250-250ML
SDS	Sigma	Cat# 75746-1KG
Methanol	VWR	Cat# BDH2018-1GLP
Tween-20	Sigma-Aldrich	Cat# P7949-500ML
GI254023X	Sigma-Aldrich	Cat# SML0789
y-Secretase Inhibitor XXI, Compond E	EMD Millipore	Cat# 565790
DMSO	Sigma-Aldrich	Cat# D2650
JaneliaFluor (JFX549)	Luke Lavis, Janelia Research Campus	N/A
JaneliaFluor (JFX646)	Luke Lavis, Janelia Research Campus	N/A
SiR-DNA	Spirochrome	Cat# SC007
Geneticin	Thermo Fisher Scientific	Cat# 10131035
Puromycin	Invivogen	Cat# ant-pr-1
Poly-D-Lysine	Thermo Fisher Scientific	Cat# A3890401
Zeba™ Spin Desalting Column	Thermo Fisher Scientific	Cat# 89882
Trizol	Thermo Fisher Scientific	Cat# 15-596-026
Critical commercial assays		
QIAprep Spin Miniprep Kit	Qiagen	Cat# 27106
PureLink™ HiPure Plasmid Filter Maxiprep Kit	Invitrogen	Cat# K210016
Dual-Luciferase Reporter Assay System	Promega	Cat# E1910
Herculase II Fusion DNA	Agilent Technologies	Cat# 600679
Taq DNA Polymerase with Standard Taq Buffer	New England Biolabs	Cat# M0273L
Platinum™ II Hot-Start PCR Master Mix (2X)	Thermo Fisher Scientific	Cat# 14000014
SU-8 2050 photoresist	Microchem, now Kayaku Advanced Materials, Inc.	https://kayakuam.com/wp-content/uploads/2019/09/SU-82000DataSheet2025thru2075Ver4-3.pdf
Lipofectamine™ 2000	Thermo Fisher Scientific	Cat# 11668019
MaXtract	Qiagen	Cat# 129056
Sylgard 184 silicone elastomer kit	Dow Corning	Cat# 2646340
FectroPro	Polyplus	Cat# 101000007
ERCC spike-in RNAs	Thermo Fisher Scientific	Cat# 4456740
DNaseI	Thermo Fisher Scientific	Cat# 18068015
ScreenTape	Agilent	Cat# 50675579
RiboZero rRNA depletion	Illumina	Cat# 20020598
Deposited data		
RNA-seq data	This paper	GEO: GSE235637
Codes used for data analysis	This paper	https://github.com/guscanavachi/Tveriakhina-Scanavachi-et-al-2024-Developmental-Cell-/tree/v1 https://doi.org/10.5281/zenodo.10790242.
Experimental models		
Human: SVG-A cells	Walter J. Atwood, Brown University	RRID: CVCL_5G13
Human: U2OS cells	Attc	Cat# HTB-96, RRID: CVCL_0042
Human: DMS53 cells	Attc	Cat# CRL-1598, RRID: CVCL_1177
Human: A673 cells	Attc	Cat# CRL-2062, RRID: CVCL_0080
SVG-A mNeonGreen-NOTCH2	this paper	N/A
SVG-A mNeonGreen-NOTCH2-HaloTag	this paper	N/A
SVG-A NOTCH2ko	this paper	N/A

(*Continued on next page*)

Please cite this article in press as: Tveriakhina et al., Temporal dynamics and stoichiometry in human Notch signaling from Notch synaptic complex formation to nuclear entry of the Notch intracellular domain, Developmental Cell (2024), https://doi.org/10.1016/j.devcel.2024.03.021

Continued

REAGENT or RESOURCE	SOURCE	IDENTIFIER
DMS53 DLL4-HaloTag	this paper	N/A
DMS53 DLL4ko	this paper	N/A
DMS53 DLL4-HaloTag, MIB1ko	this paper	N/A
A673 JAG1-HaloTag	this paper	N/A
A673 JAG1ko	this paper	N/A
Oligonucleotides		
Oligonucleotides for gene tagging, genotyping, and sequences of sgRNAs used in this study are listed in Table S1.		
Recombinant DNA		
mNeonGreen	Addgene, NeonGreen-Giantin	RRID: Addgene_98880
HaloTag	Chou et al.[58]	N/A
pX458	Addgene, pSpCas9(BB)-2A-GFP (PX458) was a gift from Feng Zhang	RRID: Addgene_48138
pX459	Addgene, pSpCas9(BB)-2A-Puro (PX459) V2.0 was a gift from Feng Zhang	RRID: Addgene_48139
pUC19	Addgene	RRID: Addgene_50005
mEos4b-N1	Addgene	RRID: Addgene_54814
pGa981-6; TP1-luc	Kurooka et al.[59]; Minoguchi et al.[60]	N/A
pRL-TK	Promega	Cat# E2231
pFUSE-hIgG1-Fc	Invivogen	Cat code: pfuse-hg1fc1
pFUSE-Jagged1ECD-hIgG1-Fc1	Martin et al.[32] this work	N/A
pET51b-10xHis-TEVsite-HaloTag	Wilhelm et al.[61]	N/A
Software and algorithms		
3D cmeAnalysis	Aguet et al.[62] Aguet et al.[63]	https://github.com/francois-a/llsmtools
FIJI	Schindelin et al.[64]	https://imagej.net/Fiji; RRID: SCR_002285
Imaris	Bitplane	Versions 8-9
MATLAB	Mathworks	RRID: SCR_001622
GraphPad Prism	GraphPad	RRID: SCR_002798
FlowJo	FlowJo	RRID: SCR_008520
A-i-O (All-in-One)	Fluigent	https://www.fluigent.com/resources-support/support-tools/software/discontinued-software/
AutoCAD	AutoDesk Corp.	N/A
Other		
8 Well chambered cover	Cellvis	Cat# C8-1.5H-N
Flow Unit M Flow-Rate Platform	Fluigent	Part number: FLU-M+
P-CAP 2 mL High Pressure	Fluigent	Cat# P-CAP2-HP-PCK
Microfluidic Flow Control System - EZ	Fluigent	Part number: MFCS™-EZ 00345001
Microfluidic Low Pressure Generator FLPG Plus	Fluigent	https://www.fluigent.com/research/instruments/pressure-sources/flpg-plus/
Tygon tubing 0.010" ID x 0.030" OD	Cole-Parmer	Cat# 06419-00
Polyurethane tubing of 0.007" ID x 0.14" OD	Instech	Cat# BTPU-014
Silicon wafers	University Wafer Silicon	ID: 447
25 mm cover slips	Glaswarenfabrik, Karl Hecht	Cat# CS-25R15
4-20% Mini-Protean TGX	BioRad	Cat# 17000928
Protran nitrocellulose membrane	Cytiva	Cat# 10600010

Please cite this article in press as: Tveriakhina et al., Temporal dynamics and stoichiometry in human Notch signaling from Notch synaptic complex formation to nuclear entry of the Notch intracellular domain, Developmental Cell (2024), https://doi.org/10.1016/j.devcel.2024.03.021

RESOURCE AVAILABILITY

Lead contact

Further information and requests for resources and reagents should be directed to and will be fulfilled by the lead contact, Stephen C. Blacklow (stephen_blacklow@hms.harvard.edu).

Materials availability

- Plasmids generated in this study are available upon request.
- Cell lines generated in this study are available upon request.

Data and code availability

- RNA-seq data have been deposited at GEO and are publicly available as of the date of publication. The accession number is GSE235637. Original western blot images, raw flow cytometry files, and raw luciferase reporter data are available upon request. Microscopy data reported in this paper will be shared by the lead contact upon request.
- All original code has been deposited at Zenodo and is publicly available as of the date of publication. The DOI is listed in the key resources table.
- Any additional information required to reanalyze the data reported in this work is available from the lead contact upon request.

EXPERIMENTAL MODEL AND STUDY PARTICIPANT DETAILS

Cell culture

SVG-A human fetal astrocytes (sex: male; RRID:CVCL_5G13), U2OS osteosarcoma (sex: female; RRID: CVCL_0042), DMS53 small cell lung carcinoma (SCLC) (sex: male; RRID: CVCL_1177) and A673 Ewings Sarcoma (sex: female; RRID:CVCL_0080) cell lines were cultured at 37°C and 5% CO_2 in DMEM supplemented with 10% heat inactivated fetal bovine serum (FBS, GeminiBio, 100-106) and 100 U/ml penicillin and streptomycin (ThermoFisher Scientific, 15140163) unless otherwise specified. All cell lines were periodically tested for mycoplasma by PCR. Cells were detached from plates after a PBS rinse using 0.05% Trypsin/0.53 mM EDTA in HBSS (Corning) for 5-10 min at 37°C unless otherwise specified.

METHOD DETAILS

Genome editing

CRISPR/Cas9 was used for genome editing to engineer doubly tagged NOTCH2 in SVG-A cells. mNeonGreen flanked by GGS (gly-gly-ser) linkers was inserted after the signal peptide of NECD; HaloTag[58] was inserted at the C-terminus of NTM after a GGAG (gly-gly-ala-gly) linker sequence and immediately before the stop codon. CRISPR/Cas9 editing was also used to insert a HaloTag at the C-terminus of DLL4 in DMS53 cells and at the C-terminus of JAG1 in A673 cells. Halo Tag was placed between a GGAG linker and immediately before the stop codon in A673 cells, or between a GGAG linker and a T2A sequence preceding a neomycin resistance cassette in DMS53 cells. Parental cell lines were seeded onto 6-well plates and transfected the next day with a mixture of repair template (8 μg) and a pX459 plasmid (4 μg) encoding the single guide RNA (gRNA) and *S. pyrogenes* Cas9 using Lipofectamine™ 2000 (Invitrogen).

Single SVG-A or A673 cells were sorted by fluorescence (mNeonGreen or HaloTag labeled with JFX646) using a SONY SH800S Cell Sorter (Sony Biotechnology) six days after transfection and collected in 50:50 conditioned:complete media (SVG-A) or 50:50 conditioned media:FBS (A673). Single colonies of DMS53 cells were obtained by selection for 30 days using DMEM supplemented with 15% FBS (Gibco, 10437028), 100 U/ml penicillin and streptomycin and G418 (1 mg/ml; Geneticin, Gibco). Colonies were manually picked and expanded. Successful tag integration in single colonies of all cell lines was detected using genome-specific primers and PCR-based genotyping. The correct sequence was then confirmed by Sanger DNA sequencing of the PCR-amplified region.

Knockout of *NOTCH2* in SVG-A cells was performed by gRNA targeting of the sequence downstream of the signal peptide in exon 2, and knockout of *JAG1* in A673 cells was carried out with two gRNAs flanking exon 1. The gRNAs were subcloned into pX458, which contains an eGFP coding sequence behind a T2A cassette downstream of the gRNA insert. SVG-A or A673 cells were transfected with the gRNA-containing plasmids using Lipofectamine™ 2000 (Invitrogen), and cells were allowed to grow for 3-6 days. Cells were then sorted for eGFP fluorescence (indicative of plasmid uptake) using a SONY SH800S Cell Sorter (Sony Biotechnology). Single SVG-A or A673 green cells were collected in 50:50 conditioned:complete media or 50:50 conditioned media:FBS, respectively. Cells were expanded and gene editing was confirmed by genotyping and Western Blot analyses. For knockout of *DLL4* or *MIB1* in DMS53 cells, two sgRNAs flanking exon1 of the target gene were subcloned into pX459 plasmids containing a puromycin resistance (puroR) gene. Cells were transfected with plasmids carrying the sgRNAs and were incubated in DMEM supplemented with 15% FBS (Gibco, 10437028), 100 U/ml penicillin and streptomycin, and puromycin (10 ug/ml) for 3 days. Puromycin was removed and single colonies were allowed to grow for 30 days. Subsequently, colonies were manually picked, expanded, and screened for DLL4 or MIB1 loss using anti-DLL4 or anti-MIB1 antibodies by Western blot and for DLL4, by flow cytometry.

All oligonucleotides used in this study are listed in Table S1.

JAGGED1-Fc expression and purification

Human JAGGED1-Fc[32] was transfected into Expi293F cells (ThermoFisher, A14527) using FectroPro (Polyplus, 101000007). Secreted JAGGED1-Fc was recovered from the culture media on Protein A agarose (Millipore, 16-125) and eluted with 100 mM glycine, pH 3.0. The eluate was neutralized with 1M HEPES buffer pH 7.3, concentrated, and buffer exchanged into 20 mM HEPES pH 7.3, containing 150 mM NaCl and 10% glycerol.

RNA-seq sample preparation

SVG-A cells were removed from plates by treating with 0.5 mM EDTA for 3 min, quenched with media, and counted. 4 x 10^5 cells per well were plated in media containing 100 nM GSI (Compound E; Millipore, 565790) on non-tissue-culture treated 6-well plates that were pre-treated overnight with PBS + 0.1 mg/ml Poly-D-lysine (Thermo Scientific, A3890401) and 200 μg/ml human JAGGED1-Fc. After 18 h, the SVG-A cells were washed three times in 4 ml of media to remove GSI, and incubated for 2, 4, or 24 hours before harvesting by resuspension in 1 ml Trizol (Thermo Scientific, 15-596-026). A "0 hr" reference control was collected by performing a mock washout with media containing 100 nM GSI and immediately harvesting in Trizol.

RNA-seq library construction

Samples in Trizol were thawed, and ERCC spike-in RNAs (Thermo Scientific, 4456740) were added at 10 μl per million cells. RNA was isolated using chloroform following the MaXtract tube protocol (Qiagen 129056). 5 μg of RNA was treated with DNaseI (Thermo Scientific, 18068015) in the presence of SUPERase-In (Thermo Scientific, AM2696). RNA quality was evaluated by HS RNA ScreenTape (Agilent, 5067-5579) on a TapeStation; all samples had RIN score > 8. 500 ng RNA was used as input for the TruSeq Stranded Total RNA sequencing kit with RiboZero rRNA depletion (Illumina, 20020598). Samples were sequenced at the Harvard University Bauer Core on a NovaSeq 6000 using the S1 300 cycle kit, with paired end 150 bp reads.

RNA-seq analysis

Reads were first mapped to ERCC spike in sequences using bowtie1.2.2 with the following parameters: -n2 -l 40 -X1000 –best -3.[65] Reads not mapping to the spike-in sequences were mapped to hg38 using STAR version 2.7.3a with the following arguments: –outMultimapperOrder Random –outSAMattrIHstart 0 –outFilterType BySJout –outFilterMismatchNmax 4 –alignSJoverhangMin 8 –outSAMstrandField intronMotif –outFilterIntronMotifs RemoveNoncanonicalUnannotated –alignIntronMin 20 –alignIntronMax 1000000 –alignMatesGapMax 1000000 –outWigType bedGraph –outWigNorm None –outFilterScoreMinOverLread 0 –outFilterMatchNminOverLread 0.[66] Reads per gene in the Gencodev33 gtf file were counted using the featureCounts function of Subread1.6.2.[67] This count matrix was used as input for DESeq2 to identify differentially expressed genes, calculating each time point versus the mock washout condition.[68] As reads mapping to the ERCC spike sequences were not different between conditions, the DESeq2 size factors were used to normalize samples.

Western blotting

Cells were rinsed with PBS, lysed in 2x Sample buffer (0.125 M Tris pH 6.8, 4% SDS, 20% Glycerol, 5% β-mercaptoethanol), sonicated and boiled at 95°C for 10 minutes. SDS-PAGE (Mini-Protean TGX, BioRad) in 0.025 M Tris, 0.2 M Glycine, 1% SDS (w/v) was followed by electrophoretic transfer to Protran nitrocellulose membrane (Cytiva) using the Mini Trans-blot wet-tank transfer system (BioRad) for 70 min at 250 mA in Transfer Buffer (0.02 M Tris, 0.223 M Glycine, 20% methanol). Membranes were stained with Ponceau Red (Fluka) to confirm successful transfer and blocked in 5% non-fat dry milk in TBS-Tween buffer (TBS-T; 20 mM Tris pH 7.6, 150 mM NaCl, 0.1% Tween-20) at room temperature. Incubations with primary and secondary antibodies were performed in TBS-T containing 5% non-fat dry milk. Signals were detected using an Odyssey CLx System (Li-Cor).

Flow cytometry

Cells were rinsed with PBS and detached from cultured plates using 0.5 mM EDTA in PBS for 5 min at 37°C and centrifuged for 4 min at 233 *g*. Cell pellets were resuspended by addition of ice-cold PBS supplemented with 2% FBS and counted using a TC-20 cell counter (BioRad). 2.5-5x10^5 cells were harvested, spun down (400 *g*, 3 min, 4°C), and dissolved in 2% FBS in PBS containing 2.5 μl antibody. Antibody incubation was performed for 1 hour at 4°C in the dark. Labeled cells were then washed 3 times with 500 μl 2% FBS/PBS and centrifuged for 3 min at 400 *g* and 4°C. Cell pellets were dissolved in 2% FBS in PBS and flow cytometry was performed using an Accuri C6 Plus (BD Biosciences) or Cytoflex Flow Cytometer (Beckman Coulter).

Luciferase Notch reporter assay

0.8x10^5 SVG-A receiver cells were seeded in each well of a 24-well plate. The following day, cells were transfected with 49 ng of a TP1-Luciferase[59,60] and 1 ng Renilla-Luciferase (pRL-TK, Promega) using Lipofectamine™ 2000 (Invitrogen) according to manufacturers instructions. 24 hours after seeding, cells were either left untreated, treated with a γ-secretase inhibitor (GSI; Compound E at 0.5 μM), an ADAM10 inhibitor (GI254023X at 5 μM) or ligand blocking antibodies (anti-DLL1 and anti-DLL4: 2 μg/ml; anti-JAG1 and anti-JAG2: 1 μg/ml). At this time, 1x10^5 sender cells were added to each well after they were detached from a TC dish using 0.05% Trypsin/0.53 mM EDTA (Corning), and counted using a TC-20 cell counter (BioRad). Approximately 24 hours after co-culture, cells

Please cite this article in press as: Tveriakhina et al., Temporal dynamics and stoichiometry in human Notch signaling from Notch synaptic complex formation to nuclear entry of the Notch intracellular domain, Developmental Cell (2024), https://doi.org/10.1016/j.devcel.2024.03.021

were rinsed with PBS, and lysed with 133 μl 1xPLB (Passive Lysis Buffer; Dual-Luciferase Reporter Assay System, Promega). 10 μl of each sample was analyzed using a GloMax Discover Microplate Reader (Promega) with 50 μl LARII (Luciferase Assay Reagent; Promega) and 25 μl Stop&Glo solution supplemented with the Stop&Glo substate (Promega).

Calibration of HaloTag^{JFX549} in solution

The concentration of N2-C (i.e., NICD) in the nucleus of SVG-A (NOTCH2) cells was estimated by using a calibration method based on 3D imaging of recombinant HaloTag protein (rHaloTag) coupled to JFX549 in solution using spinning disk confocal microscopy. rHaloTag was expressed in *E. coli*, purified as described[61] and labeled with JFX549 (the fluorophore used for visualization of N2-C). Specifically, 2 μM of rHaloTag was labeled with 8 μM JFX549 (~ 4x molar excess) in buffer solution (50 mM HEPES pH 7.3, 150 mM NaCl) for 25 min at room temperature in a total volume of 100 μl. A Zeba™ Spin Desalting Column (7K MWCO; Thermo Scientific), prewashed three times with 100 μl of buffer solution by centrifugation for 1 min at 1500 *g*, was used to remove unbound JFX549 ligand. Then, rHaloTag-JFX549 was applied to the column and centrifuged for 1 min at 1500 *g*. The flow-through was collected, the amount of rHaloTag determined by absorbance at 280 nm while the amount of JFX549 was determined by absorbance at 549 nm using a NanoDrop spectrophotometer (Thermo Scientific). A fluorescence calibration curve was then established by correlating the fluorescence intensity (F.I.) of solutions with different concentrations of rHaloTag^{JFX549} in imaging media using the spinning disk confocal microscope. Specifically, Z-stacks of 30 planes with 0.7 μm spacing between each optical plane and exposure time of 100 ms (561 nm laser) were acquired. Fluorescence intensity values from all planes were averaged and the background values obtained from imaging of the imaging media alone was subtracted. Calibration curves were obtained by fitting a linear equation to the experimental data acquired with the CCD (QuantEM, 512SC, Photometrics) or sCMOS (Prism 95B, Teledyne Photometrics) cameras (Figures S5D and S5E).

HaloTag and DNA labeling

Cells were rinsed in imaging medium (Fluorobrite DMEM; Gibco) supplemented with 5% FBS (GeminiBio), 25 mM HEPES pH 7.4 (Gibco), 2 mM GlutaMax (Gibco), and 100 U/ml penicillin and streptomycin (Gibco). Cells were subsequently incubated at 37°C for 15 min with 100 nM JaneliaFluor dye (JFX549 or JFX646, gift from Luke Lavis, Janelia Research Campus) dissolved in imaging medium, then rinsed three times with imaging medium before bathing in fresh imaging medium used during imaging. Unlabeled knockin cells, unlabeled parental cells, or JFX-labeled parental cells were imaged as controls to evaluate the specificity of HaloTag labeling. Nuclear DNA was labeled by incubating the cells for 15 min at 37°C with SiR-DNA (1:4000; Spirochrome) in imaging media during or after HaloTag labeling.

Cell delivery and cell pairing in SD microscopy

Cell delivery and cell pairing during imaging using spinning disk confocal microscopy was performed as follows: 1.5x10^4 SVG-A cells were seeded onto 8-well cover slips (Cellvis, C8-1.5H-N) to reach 30-50% confluency at the time of imaging. DMS53 cells were plated at a density of 6x10^4 cells/well in a 24-well plate. Cells were incubated overnight at 37°C and 5% CO_2 in DMEM supplemented with 10% FBS (GeminiBio, 100-106-500) and 100 U/ml penicillin and streptomycin (ThermoFisher Scientific, 15140163). The following day, plated SVG-A and DMS53 cells were labeled as described above with JFX549 and JFX646 dyes, respectively. For pairing, DMS53 cells were detached by incubation with PBS supplemented with 0.5 mM EDTA for 3 min at 37°C. Cells were transferred into 1.5 ml microcentrifuge tubes and the PBS/EDTA solution was removed by spinning down the cells for 5 min at 400-1000 *g*. The DMS53 cells were then resuspended in 200 μl imaging media and 150 μl of this solution was dispensed on top of SVG-A cells plated in the 8-well cover slips. 3D live spinning disk confocal imaging was then performed. Images of SVG-A cells, acquired before addition of the DMS53 sender cell suspension, were used as controls.

Microfluidics device

The microfluidics devices were fabricated as previously described with some modifications.[69] Briefly, photomasks were designed with AutoCAD (AutoDesk Corp.), printed by CAD/Art Services, Inc. and placed in a clean room on top of 76.2 mm silicon wafers (University Wafer, 447) to produce by photolithography 60 μm depth molds using SU-8 2050 photoresist (Microchem, now Kayaku Advanced Materials, Inc.). A 10:1 mixture of Sylgard 184 elastomer Polydimethylsiloxane (PDMS) and curing agent (Sylgard 184 silicone elastomer kit, Dow Corning) was freshly prepared, degassed for 30 min, then poured on top of the silicon wafer and spin-coated at 1000 rpm for 60 s to achieve 100 μm thickness. After degassing in vacuum for 10 min, the silicon wafer covered by the unpolymerized PDMS film was cured by incubation at 65°C for 24 hours, after which the PDMS film was peeled off and placed on top of lab tape inside a plastic petri dish. Above the sites at which the inlet / outlet tubing were later attached to the device, we placed a strip of 400-700 μm thick PDMS film bonded to the site using an air plasma cleaner (PDC-001 plasma cleaner, Harrick Plasma) at 700 mTorr, 30 W for 1.5 min followed by incubation at 60°C for 20 min. Afterwards, the PDMS film was flipped upside down and a 0.35 mm hole was punched at the tubing attachment sites using a Ted Pella puncher. The chips were plasma bonded to 25 mm diameter glass cover slips (CS-25R15 – 150 μm thickness, Glaswarenfabrik Karl Hecht) freshly cleaned by sonication for 15 min in 1M KOH followed by 3 washes in distilled water.

Tube connections to the chips were made by connecting and sealing (epoxy) polyurethane tubing of 0.007" ID x 0.14" OD (BTPU-014, Instech) into Tygon tubing of 0.010" ID x 0.030" OD (06419-00, Cole-Parmer). The polyurethane tubing was then connected to the microfluidic device and sealed with epoxy (Figure S4). Before use, the microfluidic devices were sterilized by first flowing 70%

Please cite this article in press as: Tveriakhina et al., Temporal dynamics and stoichiometry in human Notch signaling from Notch synaptic complex formation to nuclear entry of the Notch intracellular domain, Developmental Cell (2024), https://doi.org/10.1016/j.devcel.2024.03.021

ethanol through the tubing and channels and then placing the device for 5 hours in 70% ethanol. Prior to cell plating, the ethanol was removed by 5 sequential rinses with sterile PBS.

Spinning disk (SD) confocal microscopy

Cells were detached using trypsin, counted, and seeded onto 8-well cover slips (Cellvis, C8-1.5H-N) in imaging media at 37°C in presence of 5% CO_2 at densities chosen to reach 30-50% confluency at the time of imaging the following day. Images were acquired using a Zeiss Axio-Observer Z1 (Zeiss) equipped with a 63x objective (Plan-Apochromat, NA 1.4, Zeiss), a spinning disk confocal head (CSU-XI, Yokogawa Electric Corporation) with additional system magnification of 1.2x, and a spherical aberration correction system (Infinity Photo-Optical) controlled with a Marianas system (3i, Intelligent Imaging Innovation). Volumetric images were collected with 0.7 μm spacing between each optical plane and fluorescence recorded with a CCD (QuantEM, 512SC, Photometrics, 0.212 x 0.212 μm/pixel in xy) or a sCMOS camera (Prim 95B, Teledyne Photometrics, 0.145 x 0.145 μm/pixel in xy). The fluorophores were excited using solid-state lasers (Coherent Inc.) with λ excitation at 488, 561, or 640 nm coupled to an acoustic-optical tunable filter or the LaserStack (3i, Intelligent Imaging Innovation) using solid state diode lasers coupled through single mode optical fibers to the LaserStream™ (3i, Intelligent Imaging Innovation). With the CCD camera, exposure times of 100 ms in all channels were used to image membranes, Notch synapses, and nuclei; exposure times of 50 ms were used to image vesicles. With the sCMOS camera, exposure times of 60 ms were used to image signals in the 561 and 640 nm channels, exposure times of 100 ms were used in the 488 nm channel to image cell nuclei, and exposure times of 50 ms (488 nm channel), 30 ms (561 nm channel), and 60 ms (640 nm channel) were used to image vesicles.

LLSM modified with adaptive optics (MOSAIC)

Time-lapse live 3D z-stacks were acquired using a lattice light-sheet microscope modified with adaptive optics, referred here as MOSAIC (Multimodal Optical Scope with Adaptive Imaging Correction). Live cell volumetric imaging was achieved by acquiring single time points at 1 min intervals for 1 hour or longer. Sequential images spaced 0.40 μm between each plane along the z-imaging axis were obtained in sample scan mode; each time point consisted of z-stack comprised of 90-200 z-planes. Samples were illuminated with a dithered multi-Bessel lattice light-sheet[30] with 0.50 inner and 0.55 outer numerical apertures (NA) of the annular mask; lasers (MPB Communications Inc.) emitting at 488, 560 or 642 nm were used for illumination. A 0.65 NA (Special Optics) and a 1.0 NA objective (Zeiss) were used for illumination and detection using sCMOS cameras (Hamamatsu, ORCA Flash 4.0 v3) with 0.104 x 0.104 μm/pixel in xy for data visualization. Typical exposures were 50 ms for 488 nm (mNeonGreen – N2-N), 20 ms for 560 nm (HaloTag labeled with JFX549 – N2-C), and 20 ms for 642 nm (SiR-DNA or HaloTag labelled with JFX646 – DLL4).

Cell delivery and pairing for imaging in MOSAIC

$1.5x10^5$ SVG-A cells were plated onto the center of the microfluidics device, followed by overnight incubation at 37°C and 5% CO_2 in DMEM supplemented with 10% fetal bovine serum (FBS, GeminiBio, 100-106-500) and 100 U/ml penicillin and streptomycin (ThermoFisher Scientific, 15140163). Prior to imaging, the cells were labeled as described. The microfluidics device with attached SVG-A cells was then placed on the MOSAIC sample holder and its inlet tubing (Tygon tubing 0.010" ID x 0.030" OD (06419-00, Cole-Parmer)) was connected to the flow meter (Flow Unit M Flow-Rate Platform, Fluigent) (Figure S5). Another tubing, connected to a 2 ml microcentrifuge tube (Eppendorf) with an air-tight metal tube cap (P-CAP 2 mL High Pressure, Fluigent) containing a suspension of $5x10^5$ DMS53 cells labeled with JFX646, was also connected to the inlet of the flow meter. The sealed tube was further connected to the pressure controller (Microfluidic Flow Control System – EZ, Fluigent) using pneumatic tubing. The tube with suspended DMS53 cells was kept up to 5 min at 37°C (dry bath, My Block, Benchmark) before cell injection into the microfluidics device. Inlet pressure of 50-100 mbar and a flow of 10-15 μl/min for 30-90 s of the suspension containing DMS53 sender cells were controlled in real time using A-i-O software (Fluigent). Upon ending the flow, the DMS53 cells were allowed to settle by gravity and to pair with the SVG-A cells attached in the microfluidics device.

Fluorescence recovery after photobleaching

Fluorescence recovery after photobleaching (FRAP) was performed with the spinning disk confocal microscope by photobleaching a region of interest (ROI) of 1 μm in radius for 5 ms using 100% laser power. A 100 ms exposure time was used to collect images every 1 s for 10 s before bleaching and for 60 s after bleaching. SVG-A and DMS53 cells, alone or in pairs were used to perform single FRAP experiments for a given isolated cell or cell-pair. For photobleaching of synapses, 1-2 ROI were selected on the Notch synapse, while another ROI elsewhere on the cell membrane was used as a control. The position of the synapse within the ROI was determined by imaging in a non-bleached channel. A similar time series acquired in a different region of the cell not subjected to FRAP was used to correct for bleaching due to imaging only.

QUANTIFICATION AND STATISTICAL ANALYSIS

Ratiometric analysis

The relative amounts of N2-N (mNeonGreen), N2-C (HaloTag) and DLL4 (HaloTag) or JAG1 (HaloTag) associated with the Notch synapse, excluded from it and in the cell membrane, or associated with vesicles in the sender cell were determined by ratiometric analysis of the corresponding fluorescence signals within appropriate ROIs. The first step in the ratiometric analysis consisted in

Please cite this article in press as: Tveriakhina et al., Temporal dynamics and stoichiometry in human Notch signaling from Notch synaptic complex formation to nuclear entry of the Notch intracellular domain, Developmental Cell (2024), https://doi.org/10.1016/j.devcel.2024.03.021

determining the relative amount of N2-N, N2-C and DLL4 (or JAG1) within a given image. This step was achieved by comparing the fluorescence intensity of N2-N with respect to N2-C (HaloTag^{JFX549}) or N2-N with respect to DLL4 (HaloTag^{JFX549}) or JAG1 (HaloTag^{JFX549}). The second step established the relative signal resulting from JFX549 and JFX646 labeling by comparing the relative fluorescence intensity of N2-C (HaloTag^{JFX549}) in one sample with respect to N2-C (HaloTag^{JFX646}) in a second independently labeled sample.

Ratiometric analysis of fluorescence signals within appropriate ROIs was performed by using a Macro written for Fiji.[64] An ROI was defined as a portion of the object of interest (membrane, synapse, or vesicle). The fluorescence intensity of that ROI was calculated as follows: First, five consecutive planes of 0.7 μm were selected where the central plane was roughly in the center of the object of interest. Then for each plane, we drew a line intersecting the object that was three pixels in width. We took the average of the F.I. at each position along the line, and subtracted the minimum value from each average. We selected the maximum F.I. value along the line using this method, repeated this analysis for each plane, and selected the largest value among them as the F.I. of the ROI. This method was repeated for each channel to calculate the ratio. We analyzed 5-10 ROIs per cell for membrane alone, typically one ROI per synapse, and one ROI per vesicle.

FRAP analysis

FRAP analysis was conducted as described[70] using Fiji[64] on the fluorescent signal within the photobleached ROI of the Notch synapse or plasma membrane after correcting the fluorescent signals for the inherent photobleaching due to imaging; the fluorescence intensity of the first 10 time points prior to FRAP were averaged and normalized to 1. The FRAP recovery curve was fitted using a single decay exponential from which the diffusion coefficient was estimated as $D = (0.224 \times r^2)/ t_{1/2}$, where r is the radius of the bleached ROI and $t_{1/2}$ the half-life of recovery.[71]

Nuclear N2-C (i.e., NICD) concentration

The nuclear N2-C (i.e., NICD) concentration was estimated by applying the volume calibration curve to the mean nuclear NICD fluorescence intensity (F.I.) from the non-punctate and diffuse nuclear N2-C signal. A macro written using Fiji[64] was used to automate the calculations. A binary mask of the nucleus defined by the SiR-DNA signal from Notch cells was used to define the nuclear region from which to calculate the averaged intensity per plane; an estimate of the nuclear volume was obtained by multiplying the z-planes by the space between optical planes (0.7 μm). The extent of out of focus fluorescence contributed by molecules located on the plasma membrane to different z-planes within the nucleus was estimated by measuring the fluorescence of N2-C (i.e., NECD; which is always absent from the nucleus). This value was then used to correct for the contribution of out of plane N2-C signal from the plasma membrane to the nuclear signal value.

Quantification of 3D time-lapse imaged in MOSAIC

Nuclear N2-C (i.e., NICD) concentration, N2-N molecules in synapse and in DMS53 cell vesicles in the time-lapse 3D z-stacks acquired using MOSAIC was performed as follows. The fluorescence signals obtained with MOSAIC were normalized to the signals obtained with the SD. This normalization was done by determining the ratio of N2-C (HaloTag^{JFX549}) fluorescence within a plane orthogonal to the plasma membrane acquired with MOSAIC and SD. The nuclear N2-C concentration was estimated as above using SD.

A binary mask corresponding to the Notch synapse was defined by the logical Intersection of the N2-N, N2-C and DLL4 signals. The averaged N2-N fluorescence signal per pixel (0.1x0.1x0.4 μm) times the number of pixels corrected by N2-N membrane signal outside of the synapse and normalized by the signal ratio between N2-N and N2-C on the membrane corresponds to the number of N2-N (i.e., NECD) molecules in the synapse.

Vesicles containing N2-N in DLL4 cells were identified using the 3D cmeAnalysis software.[62,63] The volume of a given vesicle was defined as a box of 3x3x3 (x,y,z) pixels from which the N2-N average fluorescence and the number of molecules per vesicle were calculated as described above. This number multiplied by the number of vesicles corresponded to the total amount of N2-N trans-endocytosis into the DLL4 cell.

Statistical analysis

All statistical analyses were performed using GraphPad Prism versions 9 and 10 (GraphPad). Statistical details are indicated in the figure legends along with the exact value of n and what n represents (cells, nuclei, ROI). Sample distribution and normality tests were performed for each data set. Significance was determined using statistical tests that are included in the figures and figure legends. The MATLAB functions were built using previously published functions.[62,63]